REPORT DOCUMENTATION PAGE

Form Approved

OMB No. 0704-0188

PLEASE DO NOT RETURN YOUR FORM TO THE ABOVE ADDRESS.

1. REPORT DATE *(DD-MM-YYYY)*	2. REPORT TYPE	3. DATES COVERED *(From - To)*
08-01-2001	Final	26 Aug 99 – 25 Aug 00

4. TITLE AND SUBTITLE

"Instrumentation for Multiplex Spectroscopic Sensing"
Appendix A: "Spectroscopic Diagnosis of Chemical Processes: Applications of Optical Parametric Oscillators"
Appendix B: "Optical Heterodyne Signal Generation and Detection in Cavity Ringdown Spectroscopy Based on a Rapidly Swept Cavity"

5a. CONTRACT NUMBER
F6256299M9217

5b. GRANT NUMBER

5c. PROGRAM ELEMENT NUMBER

6. AUTHOR(S)

Dr. Brian John Orr

5d. PROJECT NUMBER

5e. TASK NUMBER

5f. WORK UNIT NUMBER

7. PERFORMING ORGANIZATION NAME(S) AND ADDRESS(ES)

Macquarie University, Dept. of Chemistry
Sydney NSW 2109
Australia

8. PERFORMING ORGANIZATION REPORT NUMBER
N/A

9. SPONSORING/MONITORING AGENCY NAME(S) AND ADDRESS(ES)

AOARD
UNIT 45002
APO AP 96337-5002

10. SPONSOR/MONITOR'S ACRONYM(S)
AOARD

11. SPONSOR/MONITOR'S REPORT NUMBER(S)
AOARD-99-04

12. DISTRIBUTUION/AVAILABILITY STATEMENT

Approved for public release; distribution is unlimited.

13 SUPPLEMENTARY NOTES

14. ABSTRACT

Identification of Project: To develop novel radiation techniques for remote spectroscopic sensing applications of interest to the USAF.

Project Objectives and Outcomes: The general technological context of this project is in the area of tunable lasers and nonlinear-optical devices that can be applied to spectroscopic sensing of gases in the atmosphere or elsewhere. This is applicable in various forms of remote sensing such as long-path absorption or DIAL/Lidar (ground-based, airborne or satellite-based). Another useful approach comprises probe-based sensing, in which a central control unit is connected optoelectronically to one or more optical probe modules that can sample traces of specific gases in industrial or environmental settings. Attainment of objectives in these areas met with mixed success. Progress on a proposed novel approach to multiple-wavelength remote sensing has been disappointingly slow, with many technical problems still to be solved. Offsetting this negative outcome is highly satisfactory progress in developing another innovative laser-spectroscopic technique that is amendable to probe-based sensing.

15. SUBJECT TERMS

Pulsed Radiation Techniques

16. SECURITY CLASSIFICATION OF:			17. LIMITATION OF ABSTRACT	NUMBER OF PAGES	19a. NAME OF RESPONSIBLE PERSON
a. REPORT	b. ABSTRACT	c. THIS PAGE			Joanne H. Maurice
U	U	U	UU	43	19b. TELEPHONE NUMBER *(Include area code)* +81-3-5410-4409

MACQUARIE
UNIVERSITY~SYDNEY

Dept. of Chemistry, Macquarie University, Sydney, NSW 2109, Australia

Phone: 61-2-9850-8289; Fax: 61-2-9850-8313

Email: brian.orr@mq.edu.au

Final Report: "Instrumentation for multiplex spectroscopic sensing"

Reference: AOARD-99-04; Contract No. F62562-99-M9217

US Air Force Office of Scientific Research (USAF OSR),
Asian Office of Aerospace Research and Development,
7-23-17 Roppongi, Minatoku, Tokyo, Japan 106-032.
MauriceJ@aoard.af.mil; HawkinsJ@aoard.af.mil

Contractor: Professor Brian J.Orr (Macquarie University, Sydney, Australia)

TABLE OF CONTENTS

		Page
1.	**INTRODUCTION**	2
1.1	Identification of project	2
1.2	Expanation of late submission	2
1.3	Project objectives and outcomes	2
2.	**PRIMARY OBJECTIVE: MULTIPLEX OPO-BASED SENSING**	3
2.1	Tunable OPO/OPA systems for spectroscopic applications	3
2.2	Spectroscopic tailoring of injection-seeded OPO output	4
2.3	A two-wavelength example: OPO CARS thermometry of furnace air	4
2.4	Progress towards realisation of a multiplex spectroscopically tailored OPO system	5
3.	**SECONDARY OBJECTIVE: PROBE-BASED CRDS SENSING**	9
3.1	Cavity ringdown spectroscopy (CRDS) – new approaches and outcomes	9
3.2	CRDS with a cw laser and a rapidly swept cavity	9
3.3	Prospects of CRDS for practical probe-based sensing	12
4.	**CONCLUDING REMARKS: PROSPECTS FOR FUTURE WORK**	12
REFERENCES		14
APPENDIX A:	G.W.Baxter, M.A.Payne, B.D.W.Austin, C.A.Halloway, J.G.Haub, Y.He, A.P.Milce, J.F.Nibler and B.J.Orr, "Spectroscopic diagnostics of chemical processes: applications of optical parametric oscillators," *Appl. Phys. B*, **71**, 651 – 663 (2000).	15
APPENDIX B:	Y.He and B.J.Orr, "Optical heterodyne signal generation and detection in cavity ringdown spectroscopy based on a rapidly swept cavity," *Chem. Phys. Lett.*, (in press; accepted for publication, 14 December, 2000).	16

1. INTRODUCTION

1.1 Identification of project

This document is the Final Report for USAF OSR project AOARD-99-04 (Contract No. F62562-99-M9217), with the following objective:

> "To develop novel radiation techniques for remote spectroscopic sensing applications of interest to the USAF. (POC: Dr Janet Fender, AFRL/VS)".

1.2 Expanation of late submission

The terms of award require the contractor to submit a detailed final report not later than 31 August 2000, with interim reports available upon request. An Interim Report was submitted on 3 December 1999, thereby securing advanced payment of the authorised fee of US$25,000.

Submission of this Final Report is therefore approximately three months overdue. This regrettable delay is due primarily to slow progress on some aspects of the project (see details below), combined with the desire to make the report as useful as possible to the USAF.

1.3 Project objectives and outcomes

The general technological context of this project is in the area of tunable lasers and nonlinear-optical devices that can be applied to spectroscopic sensing of gases in the atmosphere or elsewhere [1 – 9]. This is applicable in various forms of *remote sensing* such as long-path absorption or DIAL/lidar (ground-based, airborne or satellite-based), as depicted in Fig. 1. Another useful approach comprises *probe-based sensing*, in which a central control unit is connected optoelectronically to one or more optical probe modules that can sample traces of specific gases in industrial or environmental settings.

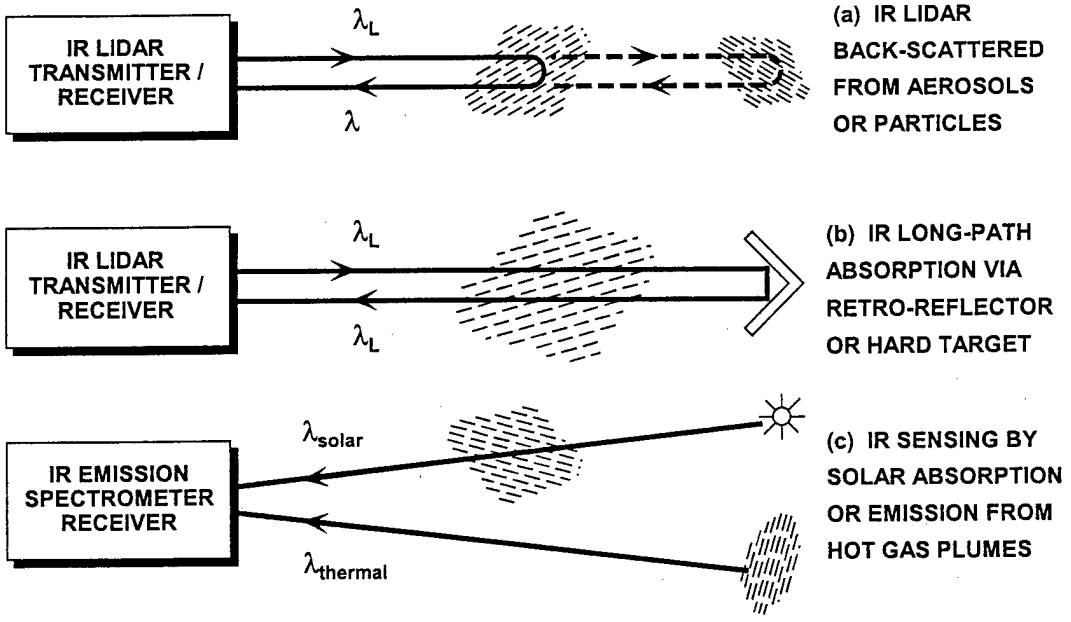

Fig. 1. IR lidar, DIAL, and related atmospheric sensing strategies (from ref. [10]).

Attainment of our objectives in these areas has met with mixed success. Progress on a proposed novel approach to multiple-wavelength remote sensing has been disappointingly slow, with many technical problems still to be solved. Offsetting this negative outcome is highly satisfactory progress in developing another innovative laser-spectroscopic technique that is amenable to probe-based sensing. Details of both of these outcomes are included in this Final Report.

2. PRIMARY OBJECTIVE: MULTIPLEX OPO-BASED SENSING

2.1 Tunable OPO/OPA systems for spectroscopic applications

Our research group at Macquarie University has developed various pulsed optical parametric oscillator (OPO) and amplifier (OPA) systems that are well suited to a range of spectroscopic sensing and imaging applications [1, 9]. We have concentrated on nanosecond-pulsed OPOs based on nonlinear-optical materials such as β-barium borate (BBO) [2 – 5, 9], KTP [3] and $LiNbO_3$ (either bulk [6] or quasi-phase-matched PPLN [7 – 9]). Injection seeding of the OPO by single-mode tunable diode lasers (TDLs) can realise very narrow optical bandwidths (≤130 MHz for PPLN OPOs [7 – 9]), approaching the Fourier transform limit of the pulse duration (~5 ns). Such TDL-seeded OPO/OPA systems, with output wavelengths ranging from near-IR (≤4 μm) to mid-UV (≥200 nm), have been applied to various forms of pulsed spectroscopic measurement.

Our most recent results in this area have been prepared and published [9] during the term of this USAF-funded project. The paper, "Spectroscopic diagnostics of chemical processes: applications of optical parametric oscillators" by Baxter *et al.* [9], is reproduced in Appendix A. It includes a report of a TDL-seeded PPLN OPO pumped by a multimode (MM) Nd:YAG laser that is more economical and compact than the single-mode (SM) lasers usually employed to pump narrowband PPLN OPOs [7, 8].

Narrowband operation of such a MM-pumped, TDL-seeded PPLN OPO depends on the resonance properties of its actively controlled ring cavity, in which the resonated wave (in this instance, the signal wave) is constrained to a single longitudinal mode that is continuously tunable without mode hops. The accompanying non-resonated wave (the idler in this case) carries the broadband character of the MM pump radiation; this is an intrinsic consequence of the energy conservation condition of an OPO.

In this way, we are able to employ a multimode pump laser and still attain single-mode tunability of signal (or idler, if that happens to be the resonated wave) output radiation. It is evident that such an MM-pumped narrowband OPO is much more readily transportable and therefore more amenable to operation in field settings for spectroscopic sensing applications requiring such coherent tunable near-IR pulses. It may therefore be of interest to the USAF. Further refinements of this approach are underway; details additional to Appendix A are available on request.

All of our recent work [7 – 9] on narrowband, TDL-seeded PPLN OPOs relies on active matching of the OPO ring cavity length to the seed wavelength by a piezolectric translator and feedback circuit, so that the signal and idler wavelengths are continuously tunable without mode-hops [8]. This approach can yield single-mode output with good beam quality and small optical bandwidth, but it is complicated optically and electronically and is unsuitable for multi-wavelength spectroscopic tailoring.

2.2 Spectroscopic tailoring of injection-seeded OPO output

The primary objective of this project has been to develop pulsed OPO/OPA systems that are injection-seeded by a multi-wavelength source to generate "spectroscopically tailored" sets of output wavelengths under computer control. Highly sensitive species detection is then expected *via* a spectrocopic multiplex advantage that arises by particularly selecting coherent radiation only at wavelengths that offer optimum information content and by using coded sequences of such wavelengths.

The central technology in this context is that of *pulsed OPOs with low-finesse cavities* that facilitate simultaneous narrowband injection seeding at a number of specific signal or idler wavelengths.

Pump radiation for such an OPO system is typically generated by a single-mode Nd:YAG laser, all-solid-state, high-repetition-rate versions of which are now commercially available. In contrast to our narrowband tunable PPLN OPOs, where *active control* of OPO cavity length is needed [7 – 9], simultaneous multi-wavelength injection seeding employs *passive control* of an OPO cavity in which one reflector is slightly misaligned (by ~2 mrad) to give it a low effective finesse and a continuous range of acceptable seed wavelengths. It enables continuous tuning of the injection-seeded OPO signal and idler outputs as the TDL seed wavelength is scanned. This occurs without mode hops and without locking OPO cavity length to TDL wavelength. This is simpler optically and electronically than active control of the OPO cavity; in either case, the narrowband tuning tracks the TDL seed wavelength.

We have explored this passive, misaligned-cavity approach extensively [1 – 6, 9]. It is understood [3] to depend on the high Fresnel number (~100) of the OPO cavity used, with transverse-mode spacings much less than the Fourier-transform limit for the optical bandwidth of the pulsed radiation generated. This introduces higher-order transverse modes, thereby smoothing out the sparse distribution of resonances that occur when the OPO cavity is well aligned. A resulting disadvantage is that the multiple transverse modes result in a degradation of output beam quality, but not impossibly so. Moreover, it proves difficult to eliminate a low-intensity broadband "pedestal" that tends to accompany the narrowband tailored wavelength components; even when this pedestal is very weak, it can degrade the detection sensitivity, specificity and linearity of some forms of spectroscopic sensing [9].

As already noted, the passive-cavity approach is unsuitable for TDL-seeded OPOs based on quasi-phase-matched media such as PPLN [7, 8]. However, it is essential for multi-wavelength spectroscopic tailoring [4, 5] by injection seeding of birefringently phase-matched bulk OPO media.

A second key technology for spectroscopically tailored OPOs is *multi-wavelength injection seeding* by a set of single-mode tunable diode lasers (TDLs), as either discrete components or a monolithic array.

The ultimate spectroscopic tailoring capability would be *via* 2-dimensional rastered multi-wavelength arrays of VCSELs (vertical-cavity surface-emitting lasers); such devices have been developed [11] but are still not routinely available. Meanwhile, we continue to employ discrete single-mode TDLs, either external-cavity diode lasers that are continuously tunable [4, 5] or DBR (distributed Bragg reflector) diode lasers that are settable to a particular single-mode wavelength.

2.3 A two-wavelength example: OPO CARS thermometry of furnace air

A two-wavelength version of the spectroscopic tailoring approach has already been demonstrated in our earlier work [4, 5] on multiplex coherent anti-Stokes Raman spectroscopy (CARS). A TDL-seeded BBO OPO has been used for thermometry of nitrogen in furnace air, as shown in Figs 2 and 3 (which have not previously been published [12]). CARS signals are detectable in a single 5-ns OPO shot and so are insensitive to turbulence – a significant advantage for combustion diagnostics.

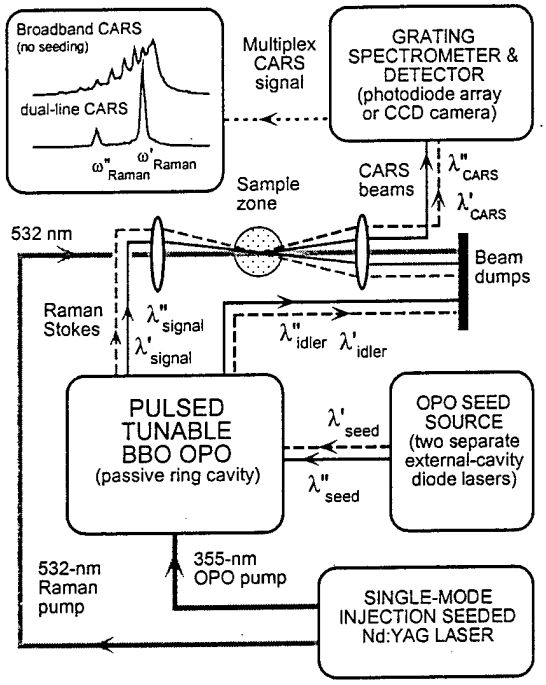

Fig. 2. Schematic of a spectroscopic system for dual-line OPO CARS measurements (from ref. [12]).

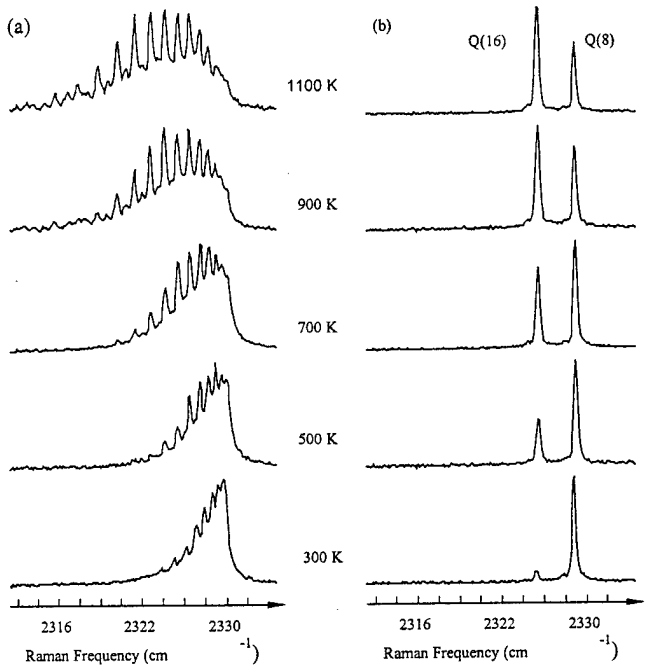

Fig. 3. Broadband (a) and dual-line (b) OPO CARS measurements of nitrogen (N_2) in furnace air, *via* the 2330-cm^{-1} Raman Q branch (from ref. [12]).

2.4 Progress towards realisation of a multiplex spectroscopically tailored OPO system

Our ability to tailor multi-wavelength narrowband output from a single pulsed, tunable coherent OPO source could be particularly attractive for remote spectroscopic sensing (*e.g.*, by long-path absorption in industrial and environmental settings or by satellite-based or airborne DIAL/lidar surveillance). We expect to realise high sensitivity and specificity by matching the spectrum of the OPO radiation to that of a particular sample or target species, as illustrated above by Figs 2 and 3.

To optimise the detection sensitivity and specificity attainable *via* the technique's multiplex advantage, it is necessary for each narrowband component of the set of spectroscopically tailored OPO output wavelengths to be computer-controllable and capable of modulation in ways that enable subsequent demodulation or decoding of the resulting spectroscopic signals. This modulation is achievable by some form of computer-controlled optical switch (*e.g.*, a multichannel fiber-optic switch).

The conceptual layout of such a spectroscopically tailored OPO system configured for multiplex IR DIAL lidar measurements is illustrated in Fig. 4 below.

As foreshadowed in the Interim Report (December 1999) and outlined above, our intention is to employ a set of several discrete single-mode DBR diode lasers operating at ~852 nm, each separately temperature- and current-controlled. Each narrowband component of the set of spectroscopically tailored wavelengths must be computer-controllable and capable of modulation (*e.g.*, by switching successive characteristic wavelengths in and out of resonance from one OPO shot, or burst of shots, to the next) in ways that enable subsequent demodulation or decoding of the resulting spectroscopic signals, thereby obtaining a multiplex advantage for detection sensitivity and specificity.

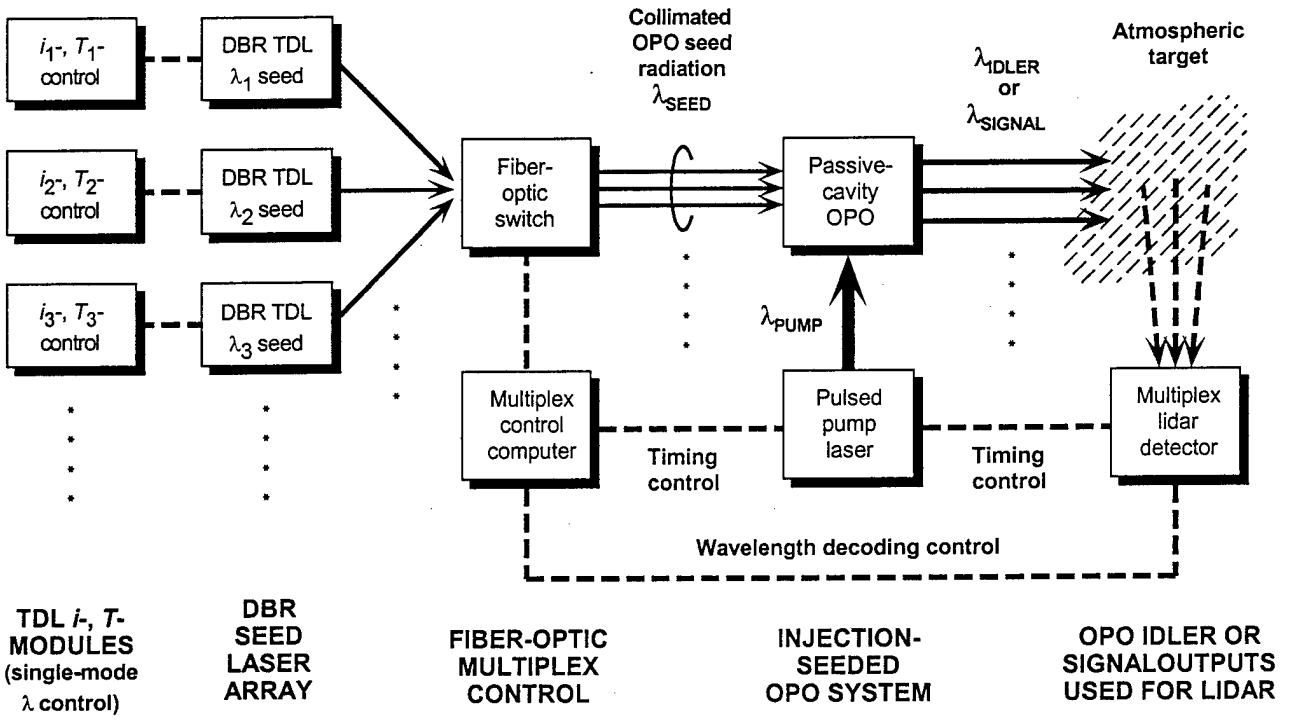

Fig. 4. Proposed schematic of a spectroscopically tailored multi-wavelength IR DIAL system [10].

During the course of this USAF-funded project, we have acquired virtually all of the optical, electronic and mechanical components needed to demonstrate this concept. Various sections of the multi-wavelength OPO system have been tested and refined, but much remains to be done before it will be fully operational. A summary of the major components is presented in Table 1. Following that, we add some explanatory comments and identify a few substantial setbacks that have been encountered.

Table 1. Major components of a spectroscopically tailored multiplex BBO OPO system

Component	Description and comment(s)
Nd:YAG pump laser (single-mode, Q-switched, 355 nm)	*Either* S-P GCR-250 (lamp-pumped) ⇒ ~200 mJ per 8-ns pulse @ 10 Hz *or* CEO CT-series (diode-pumped) ⇒ ~1 mJ per 22-ns pulse @ 1 kHz.
TDL-seeded BBO OPO design	Passive 3-mirror misaligned cavity; signal @ ~608 nm (cavity-resonant); idler @ ~ 852 nm (TDL-seeded); see refs [1 – 5, 9] for specifications.
TDL injection seeding units	SDL 5702-H1 DBR single-mode GaAsAl TDLs ⇒ ~10 mW cw @ ~852 nm.
TDL multiple-wavelength controller	Newport 8008-OPT 8-channel mainframe unit with GPIB interface and up to eight 8605.8C combined current / temperature controller plug-in modules.
Multiplex OPO injection-seeding configuration	Up to eight DBR lasers, fibre-coupled to a common OPO injection-seeding axis, each piezoelectrically switched for multiplex coding; see text for details.

At present, the pump laser available for the passive-cavity BBO OPO [1 – 5, 9] is one of several large flashlamp-pumped, single-mode Nd:YAG lasers (*e.g.*, Spectra-Physics GCR-250 or GCR-5, each with Lightwave S-100 injection seeder and HG-4 third harmonic generator) in our laboratory. By February 2001, we expect to install a new all-solid-state, diode-pumped Nd:YAG laser that has been custom-built for us by Cutting Edge Optronics, Inc. (CEO; St Charles, MO) *via* an order originally placed with Continuum Electro-Optics, Inc. (Santa Clara, CA) in February 1999. It is injection-seeded for single-mode operation with relatively long pulse duration (>20 ns fwhm) and high repetition rate (1 kHz). Moreover, it is more compact and transportable than existing flashlamp-pumped counterparts. Progress on this USAF-funded project has been inhibited by several critical failures of our flashlamp-pumped Nd:YAG lasers and by long delays in the design and construction of the special CEO laser.

The general design of the passive-cavity BBO OPO system is well established [1 – 5, 9] and we have studied performance characteristics (some not yet published [12]) that enable it to be used for spectroscopic tailoring by multi-wavelength injection seeding. More development effort is needed in introducing the CEO Nd:YAG laser to pump the BBO OPO, since its pulse energy is much lower and its repetition rate much higher than with current flashlamp-pumped Nd:YAG lasers. We are likely to need to use tighter focusing and higher OPO-cavity-mirror reflectivities to attain BBO OPO threshold conditions.

All of our previous work [2 – 5, 9] with a TDL-seeded BBO OPO has employed continuously tunable external-cavity diode lasers for injection seeding. In the present project, we prefer to use less elaborate, more compact DBR (distributed Bragg reflector) diode lasers. These are not as easy to tune continuously without mode hops, but they can readily be set to a specific (single-mode) wavelength by control of temperature (@ 0.07 nm/C°) and injection current (@ ~0.003 nm/mA). Such wavelength control is provided by a commercially available 8-channel controller (Newport 8008-OPT with 8605.8C plug-in modules; see Table 1) with digital interface. The injection-seeding wavelength range for the proof-of-principle stage of this project is determined by the commercial availability of DBR lasers: namely, SDL model 5702-H1 GaAsAl laser diodes emitting at 852 ± 1 nm.

Such DBR injection seeding determines the idler output wavelength of a 355-nm-pumped BBO OPO, so that the corresponding signal output wavelength is 608.6 ± 0.6 nm. Alternatively, for a 532-nm-pumped OPO (based on $LiNbO_3$, KTP or BBO), the DBR and signal wavelengths would coincide and the idler output wavelength would then be 1416 ± 3 nm.

Fig. 4 depicts the use a multichannel fiber-optic switch system to direct the injection-seeding radiation from the DBR diode lasers to the OPO. Such a unit was sourced from JDS-Uniphase (Model SA-Z421, including GPIB/RS232 interface), but was considered to be not cost-effective at ~US$15,000. A simpler, cheaper approach is being adopted as an alternative, as explained below.

The available SDL 5702-H1 DBR lasers do not have fiber-optical pigtail connectors, so that we need to use discrete optics (Newport F-915T with M-10X microscope objective) to focus each DBR laser output beam separately into an optical fiber (Newport F-SBA, single-mode, 4.1-μm core). Up to eight of these fibers (one for each of the DBRs) can then bundled together and the output injection-seeding light imaged collinearly into the BBO OPO ring cavity. The discrete optical coupler stage will enable each injection-seeding channel to be modulated ("on" or "off") from one OPO shot (or burst of shots, in the case of a 1-kHz repetition rate) to the next. This modulation control can be achieved simply by inserting a low-voltage piezoelectric translator (PZT) to displace the fiber in and out of the focus of the objective lens of each of the optical couplers; the above two modulation logic levels then correspond to switching the voltage applied to each PZT "on" or "off". A suitable PZT for this purpose is available from Thorlabs (model AE0203D08; 6-μm displacement @ 100 V; 138-kHz resonance frequency).

To appreciate the way in which we intend to code the modulated sequence of injection-seeder stimuli and to decode the corresponding responses by single-channel (*i.e.*, non-dispersive) detection system to the OPO radiation, consider the following hypothetical example. Suppose that we investigate a gas-phase target containing two known molecular species (A and B) at a known temperature, each with two characteristic spectral features (A1, A2 and B1, B2) and corresponding background/baseline points (A1*, A2* and B1*, B2*). Each of the eight DBR lasers is tuned to and fixed at the central wavelength of each of these features. To monitor relative concentrations of species A and B, it is useful to record detected amplitudes corresponding to the following linear combinations: (A1 + A2) – (A1* + A2*) and (B1 + B2) – (B1* + B2*), by using a repetitive four-shot sequence of OPO outputs for A1 and A2 (simultaneously), then A1* and A2*, then B1 and B2, then B1* and B2*. Likewise, detected amplitude ratios such as (A1 – A1*)/(A2 – A2*) or (B1 – B1*)/(B2 – B2*) will generally provide information on local temperatures (rotational or vibrational, depending on which pairs of spectral features are chosen). It will be straightforward for the computer that controls the coding (*i.e.*, which shot contains which spectroscopically tailored wavelengths) to control the decoding and thereby generate the desired linear combinations and/or ratios of detected amplitudes. The data-processing approach is similar in some respects to that employed in Hadamard transform spectroscopy [13], a form of multiplex spectroscopy where two-dimensional masks (one of them translatable sideways) replace the entrance and exit slits of a conventional dispersive optical spectrometer.

One of our immediate objectives is to conduct laboratory-based spectroscopic measurements with the new multi-wavelength BBO OPO system to demonstrate the feasibility and advantages (or otherwise) of our spectroscopic tailoring concept. The available idler output wavelength range of 852 ± 1 nm corresponds to wavenumbers of 11737 ± 14 cm^{-1}. This is suitable for high-overtone absorption spectroscopy of certain molecules in the gas phase, combustion media or supersonic free jets (*e.g.*, by photoacoustic absorption or cavity ringdown methods [9]). For instance the R branches of two high-order rovibrational combination bands of acetylene (C_2H_2) fall in this region: $(0312^02^0) – (0000^00^0)$ centered at 11707 cm^{-1} and $(0221^11^1) – (0000^00^0)$ centered at 11 717 cm^{-1} [14].

Subsequent field-based spectroscopic sensing will be a later feature of this project's research agenda, once our long-awaited 1-KHz CEO Nd:YAG laser has been commissioned.

We now summarise factors that have contributed to the relatively slow progress of this USAF-funded project. Some of them have already been mentioned in passing; others have not. They are as follows:

- Several failures (*e.g.*, power supplies and injection seeders) of flashlamp-pumped Nd:YAG lasers.
- Extended delays (approaching two years!) in delivery of the all-solid-state, diode-pumped Nd:YAG laser required for field-based sensing and/or high-repetition-rate measurements.
- Indecision (resolved as above) as to how to modulate the multiple-DBR injection-seeding input.
- A shortfall in research funds for this and closely related projects (we were awarded only ~25% of Australian research grants requested for the triennium commencing 2000).
- A general shortage of research students with all recent graduate students from our laboratory going directly to employment in the local telecommunications/photonics industry, rather than considering further university-based graduate or postdoctoral research.
- A corresponding shortage of suitably qualified postdoctoral research staff, for similar reasons.
- Concentration of available personnel on other promising research projects (*e.g.*, see Sec. 3 below).

These factors may help to explain why progress on this project has been slower than first projected, alongside technical and scientific information on steps that we have taken towards a workable system.

3. SECONDARY OBJECTIVE: PROBE-BASED CRDS SENSING

3.1 Cavity ringdown spectroscopy (CRDS) – new approaches and outcomes

Probe-based sensing, with one or more optical probe modules optoelectronically connected to a central control unit, was identified in Sec. 1.3 above as a useful alternative to regular remote sensing in some applications that may be of interest to the USAF. During the term of this USAF-funded project, significant progress has been made in developing novel cavity ringdown spectroscopy (CRDS) techniques that are amenable to probe-based sensing. Such outcomes are therefore included in this Final Report, even though they were not within the original terms of reference.

CRDS is now well established as a highly sensitive way to use lasers to measure molecular absorption spectra [15, 16]. The technique employs narrowband coherent radiation, either pulsed or continuous-wave (cw), to examine samples contained in a high-finesse optical cavity. Information is obtained by measuring temporal responses rather than variations of optical intensity. CRDS with pulsed lasers is straightforward and popular [9] (*e.g.*, see Appendix A), but cw versions of CRDS are favored in order to attain superior spectroscopic resolution or to take advantage of cheap, compact TDL sources.

In previous work [17], we have demonstrated a novel variant of cw-CRDS, in which the length of the optical cavity is swept, continuously and rapidly, through resonance with narrowband TDL radiation. This facilitates growth and subsequent decay ("ringdown") of optical energy in the cavity and yields absorption spectra with high sensitivity and with minimal instrumental complexity and cost. In particular, it avoids the inherent complexity and expense of an electro-optic or acousto-optic switch, as is needed in conventional cw-CRDS methods.

More recently [18, 19], we have developed a novel optical-heterodyne detected (OHD) extension of cw-CRDS with a rapidly swept ringdown cavity. This OHD approach is highly sensitive and simple to implement with a commercially available TDL system. In contrast to other more elaborate OHD designs for cw-CRDS [16], it does not need a separate optical switch or modulator, nor is it necessary to lock the ringdown cavity length and laser wavelength to each other or to use a laser that is specially stabilised and/or modulated.

A preprint of the paper, "Optical heterodyne signal generation and detection in cavity ringdown spectroscopy based on a rapidly swept cavity" by He and Orr [18], is reproduced in Appendix B. Some key results are presented in the following section.

3.2 CRDS with a cw laser and a rapidly swept cavity

Fig. 5 depicts our cw-CRDS apparatus, applicable to either direct (forward-transmitted) [17] or OHD (back-reflected) [18] operational modes. Each of these two cw-CRDS approaches, in which cavity length is swept rapidly and continuously by means of a PZT, depends on the dynamic response of cw coherent radiation in an optical cavity. A tiny cavity mirror displacement (~1 nm) suffices to shift such a high-finesse (typically, $F > 10^4$) cavity on and off resonance. Optical energy is built up and stored in the cavity as any of its modes moves into resonance with the laser wavelength, and the cavity then transmits much more light. The input light is effectively blocked by the highly reflective cavity mirrors once the swept cavity has moved off resonance; the light stored in the cavity during the build-up period then decays gradually with a ringdown time constant τ that depends on mirror reflectivity and the absorption of the optical medium inside the cavity. The temporal profile of the forward-transmitted light intensity is then asymmetric, with a slowly decaying tail that exhibits characteristic ringing due to interference of the multiply reflected, Doppler-shifted intracavity light, as can be seen in Figure 6(a).

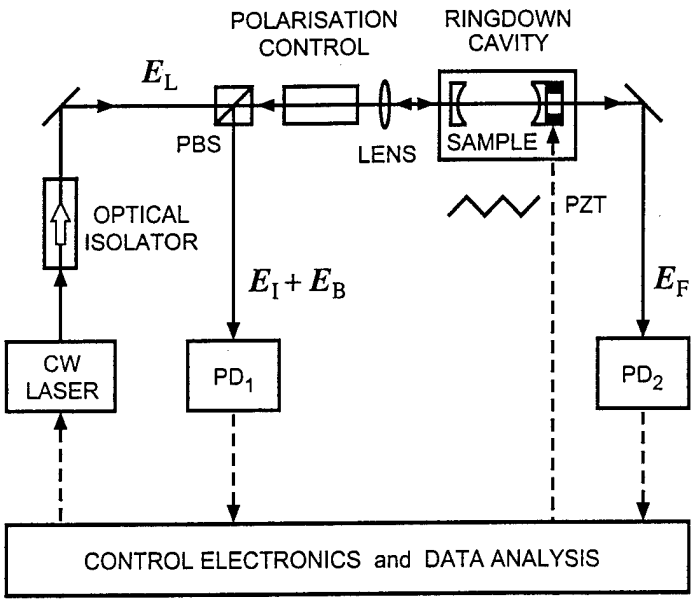

Fig. 5. Schematic of OHD cw-CRDS apparatus with an optical cavity whose length is swept rapidly and continuously by a PZT. Photodetectors PD_1 and PD_2 monitor OHD (back-scattered, "$\boldsymbol{E}_I + \boldsymbol{E}_B$", *via* polarising beam splitter, PBS) and direct (forward-scattered, "$\boldsymbol{E}_F$") ringdown signals, respectively. Taken from ref. [18].

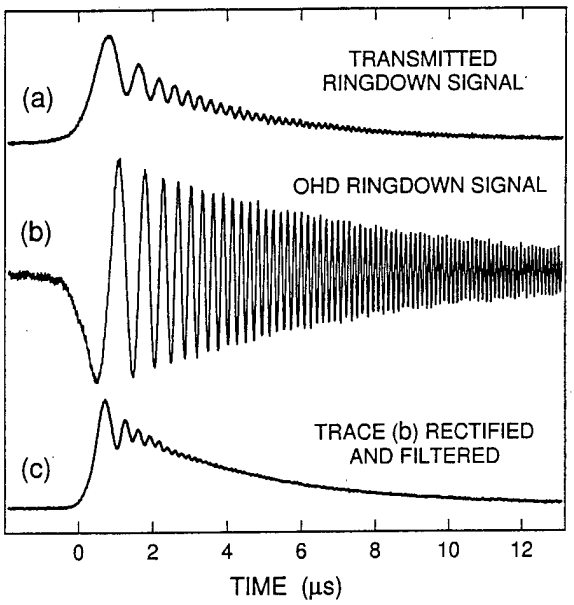

Fig. 6. Simultaneously recorded cw-CRDS signals showing the dynamic response of cw coherent radiation in a rapidly swept optical cavity: (a) forward-scattered signal (PD_2); (b) raw OHD signal (PD_1); (c) rectified and filtered waveform. Taken from ref. [18].

Figs 5 and 6 also depict the mode of operation of our recently introduced [18, 19] OHD cw-CRDS. This approach is a highly sensitive and simple extension of our earlier directly detected method [17]. In both cases, we use a commercially available TDL and a rapidly swept ringdown cavity.

Fig. 5 shows light emerging from the cavity both through both the moving *back* mirror (electric radiation field $\boldsymbol{E}_F$, detected by PD_2) and through the stationary *front* mirror ($\boldsymbol{E}_B$). Most of the incident laser field ($\boldsymbol{E}_L$) is reflected back off the front mirror of the cavity; that reflected laser light field $\boldsymbol{E}_I$ co-propagates with $\boldsymbol{E}_B$ and both can be monitored by PD_1 *via* a polarising beam splitter. Doppler-type frequency shifts associated with the moving cavity mirror cause $\boldsymbol{E}_I$ and $\boldsymbol{E}_B$ to differ in optical frequency, so that OHD signals are straightforwardly obtained as they beat against each other and generate heterodyne signals at PD_1. The $(\boldsymbol{E}_I^* \cdot \boldsymbol{E}_B)$ heterodyne cross term contains a slowly varying exponential decay factor that depends on the cavity ringdown time τ. A significant amplification factor arises because the field $\boldsymbol{E}_I$ is much stronger than $\boldsymbol{E}_B$ or $\boldsymbol{E}_F$. Detection sensitivity is further enhanced by the fact that the OHD (PD_1-monitored) signal decays twice as slowly as the direct (PD_2-detected) ringdown signal. Moreover, the higher frequency domain of the OHD signal facilitates high-pass filtering to reduce low-frequency technical noise.

Fig. 6(b) shows the outcome of the PD_1-detected OHD cw-CRDS approach [18, 19], compared with the direct (PD_2-detected) outcome [17] shown in Fig. 6(a). All three traces of Fig. 6 are recorded simultaneously, as the cavity length is swept rapidly and continuously by a ramp voltage applied to the PZT that bears one of the mirrors. To extract the ringdown decay rate τ^{-1} from the PD_1-detected OHD

signal shown in Fig. 6(b), we use simple analog circuity to rectify that signal and smooth the oscillatory part with a filter time constant that is much smaller than the ringdown time τ. This yields a smooth, single-exponential decay curve, as depicted in Fig. 6(c). Ringdown times τ can be accurately and rapidly derived from decay envelopes such as Fig. 6(a) or 6(c) while spectra are being scanned.

CRDS measurements typically comprise plots of the rate constant τ^{-1} for energy loss from the cavity as the laser wavelength is scanned. Two examples of such spectra are shown in Figs 7 and 8 below. They comprise rovibrational IR absorption spectra of carbon dioxide (CO_2) gas around ~1.53 μm, where several weak high-order combination and hot bands overlap. The lower plot of Fig. 7 is a directly detected cw-CRDS scan [17] over a spectral range of ~40 cm^{-1}; it corresponds closely to a simulation (upper plot) from the HITRAN '96 database [20]. Fig. 8 shows a finely resolved OHD cw-CRDS trace in the vicinity of the Q branch of the 6538-cm^{-1} $(11^12)_{II}$ – (00^00) combination band [20, 21] of CO_2 gas (P = 50 mbar, T = 296 K); the linewidths (0.018 cm^{-1} FWHM) are determined by a combination of Doppler and pressure broadening. Fig. 8 provides a "zoom" view (1.3 cm^{-1} wide) of the congested 6538-cm^{-1} Q-branch region that is barely discernible in Fig. 7.

The noise-limited sensitivities for absorption detection obtained in Figs 7 (direct cw-CRDS) and 8 (OHD cw-CRDS) are 7 x 10^{-8} cm^{-1} and 3 x 10^{-9} cm^{-1}, respectively, which compare favorably with other forms of CRDS. Despite the fact that these are very weak absorption bands of CO_2 [20, 21], minimum detection limits of ~20 ppm (diluted in air and allowing for pressure broadening) can be realised.

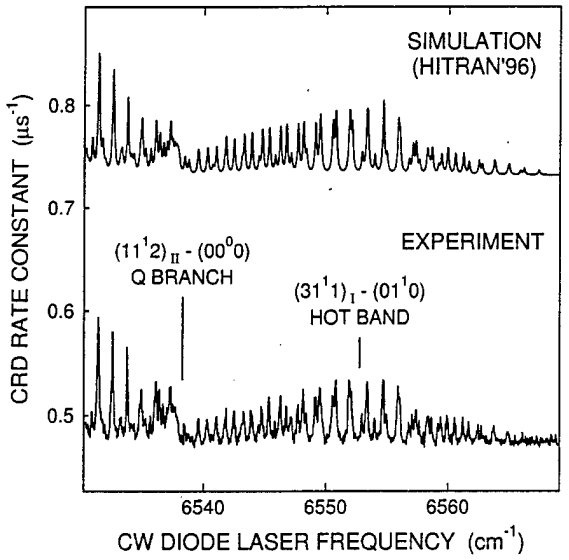

Fig. 7. Rovibrational IR absorption spectra at ~1.53 μm for a gas mixture of CO_2 and N_2 with P_{CO_2} = 0.20 bar, P_{N_2} = 0.80 bar, and T = 296 K. A directly detected cw-CRDS trace (lower plot) is compared with a simulation (upper plot) from the HITRAN '96 database [20]. Taken from ref. [17].

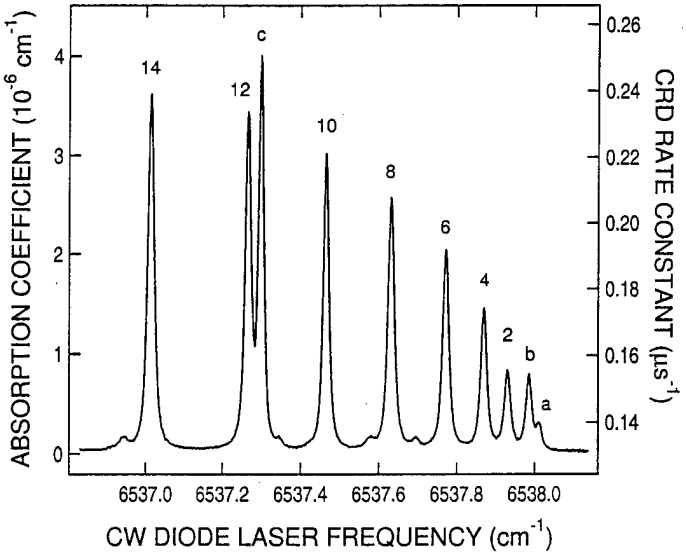

Fig. 8. OHD cw-CRDS scan at ~1.53 μm of CO_2 gas at 50 mbar in a rapidly swept optical cavity. The spectrum records very weak rovibrational IR absorption bands of CO_2, including the Q(J) features of the 6538-cm^{-1} $(11^12)_{II} \leftarrow 00^00$ band, with J = 2 – 14 and others (a, b, c) that are assigned by the HITRAN'96 database [20, 21]. Taken from ref. [18].

3.3 Prospects of multiplex CRDS for practical probe-based sensing

It is evident from Sec. 3.2 that our use of a rapidly swept cavity for either direct [17] or OHD [18, 19] cw-CRDS yields high spectroscopic resolution, accuracy, and sensitivity. This enables a relatively simple external-cavity single-mode TDL to be used, thus avoiding pulsed Nd:YAG lasers and OPOs. Technical improvements should be feasible, without sacrificing intrinsic simplicity, low cost, and compactness of our techniques. It is clear from ref. [19] that we are taking steps to commercialise our inventions if possible. At present, however, cw-CRDS is still a laboratory-based technique in which spectra are recorded by slowly scanning laser wavelength. We need to go beyond this.

Our results offer the prospect of compact, transportable instruments for spectroscopic sensing in the field or at industrial sites. In particular, the swept-cavity OHD cw-CRD technique [18, 19] should be amenable to optical-fiber-coupled systems with the ringdown cavity remotely located relative to the TDL and detection system, thereby facilitating environmental monitoring applications. We have already taken some first steps in this direction, with encouraging results. We envisage a system comprising one or more small sensor modules, each comprising a ruggedised ringdown cavity with inlet and outlet ports for gas sampling and an "umbilical cord" (containing optical fiber, PZT voltage cable and other connections to sensor-based temperature and pressure gauges, etc.) connecting it to a central control unit containing most of the optical, electronic and computing instrumentation needed. Such an arrangement would be compatible with certain forms of robotically mounted sensing.

We are also working on multiplex cw-CRDS techniques to collect real-time, instantaneous spectroscopic information at more than one characteristic wavelength. Many of the spectroscopic tailoring concepts applied in Sec. 2.4 to sensing with a multi-wavelength TDL-seeded OPO system could be equally applicable here. In a recent primitive demonstration of multiplex cw-CRDS [22], two separate DFB lasers, each with a separate acousto-optic modulator (AOM), were coupled to a ringdown cavity *via* a single-mode optical fiber and used for multiple-species detection. Our variant of cw-CRDS removes the need for AOMs and offers the prospect of using more than two DFB lasers fiber-coupled to a rapidly swept high-finesse cavity, with each laser wavelength giving rise to a distinct ringdown waveform (as in Fig. 6) at different points in the cavity-sweep cycle.

4. CONCLUDING REMARKS: PROSPECTS FOR FUTURE WORK

Sec. 2 of this Final Report contains a body of results that are incomplete at this stage, concerning a multi-wavelength TDL-seeded pulsed OPO system intended for spectroscopic remote sensing as initially envisaged at the outset of this project.

In addition, Sec. 3 contains unsolicited information about probe-based spectroscopic sensing methods based on cw-CRDS with a rapidly swept optical cavity, which has yielded particularly promising results during the term of this USAF-funded project.

The instrumentation that is under development so far is constrained by the commercial availability of components such as communications-band TDLs (*e.g.*, DBRs at ~852 nm), optical fibers, high-reflectivity mirrors (*e.g.*, for high-finesse ringdown cavities) and nonlinear-optical materials (*e.g.*, for OPOs). This is adequate to establish proofs of principle and/or technological feasibility, but actual spectroscopic sensing applications that are likely to be of interest to the USAF would probably need to have access to more specialised optical and electronic components. For instance, a specific USAF-driven sensing application might encourage fabrication of specially designed 2-dimensional multi-wavelength rastered VCSEL arrays [11] for OPO injection-seeding or multiplex cw-CRDS operations.

It is hoped that the USAF OSR will continue to have an interest in our ongoing research in the general area of this project. Future research that could be undertaken in this context is as follows:

(i) Completion of laboratory-based trials of the spectroscopically tailored OPO concept, to provide a spectroscopic proof of principle (*e.g.*, *via* IR spectra of C_2H_2 at ~852 nm, as proposed on p. 8).

(ii) Extension of item (i) above to a transportable multiplex pulsed OPO system (*e.g.*, pumped by the CEO laser), capable of field trials to establish feasibility of genuine remote sensing applications.

(iii) Further development of the MM-pumped narrowband PPLN OPO system [9] as a compact, low-cost source of pulsed, coherent, tunable near-IR radiation for spectroscopic sensing applications.

(iv) Refinement of OHD cw-CRDS with a rapidly swept optical cavity [18, 19], with particular emphasis on its potential as a fiber-coupled probe-based sensing technology.

(v) Development of DFB-based multiplex variants of the OHD cw-CRDS technique as in item (iv), using spectroscopic tailoring principles similar to those proposed for OPOs in items (i) and (ii).

Inadequate progress of the originally commissioned portion of this project indicates that the degree of difficulty of some aspects of its objectives had been underestimated at the outset. We should be more conservative in future!

Of the difficulties identified at the end of Sec. 2.4 (p. 8), levels of research funding that are substantially below what had been requested from Australian research funding agencies have not so far severely limited our rate of progress, in view of our accumulated reserves and the much-appreciated USAF OSR grant of US$25,000. However, further work along the lines proposed above will require financial support from sources other than local government research agencies. It is hoped that there will be continued USAF OSR interest and financial support (despite our imperfect track record in this initial instance). To develop our cw-CRDS innovations (*e.g.*, by licensing our patent [19]), we are also seeking support from companies in the USA (rather than in Australia, given its limited market scale).

In the immediate future, our research group at Macquarie University faces a severe shortage of well-qualified personnel to work on its various ongoing projects. The migration of research students and postdoctoral staff into the private R&D sector (notably the buoyant fields of telecommunications and photonics, for which our people are particularly well trained) has no obvious remedy as far as Australian university-based research is concerned. A fresh recruitment campaign will resume in the near future, aiming to replenish the long-established strength of the research group.

Finally, a major share of the credit for the progress described in this Report must be attributed to Dr Yabai He (Research Fellow). He has been the prime mover behind virtually all of our innovative scientific and technological developments over the last few years [7 – 9, 17 – 19].

REFERENCES

[1] B.J.Orr, M.J.Johnson and J.G.Haub, "Spectroscopic applications of tunable optical parametric oscillators," Chapter 2 in *Tunable Laser Applications* (ed. F.J.Duarte; Marcel Dekker, New York, 1995; ISBN 0-8247-8928-8), pp. 11 – 82.

[2] M.J.Johnson, J.G.Haub and B.J.Orr, *Opt. Lett.*, **20**, 1277 – 1279 (1995).

[3] J.G.Haub, R.M.Hentschel, M.J.Johnson and B.J.Orr, *J. Opt. Soc. Am. B*, **12**, 2128 – 2141 (1995).

[4] G.W.Baxter, M.J.Johnson, J.G.Haub and B.J.Orr, *Chem.Phys. Lett.*, **251**, 211 – 218 (1996).

[5] G.W.Baxter, J.G.Haub and B.J.Orr, *J. Opt. Soc. Am. B*, **14**, 2723 – 2730 (1997).

[6] G.W.Baxter, H.-D.Barth and B.J.Orr, *Appl. Phys. B*, **66**, 653 – 657 (1998).

[7] G.W.Baxter, Y.He and B.J.Orr, *Appl. Phys. B*, **67**, 753 – 756 (1998).

[8] Y.He, G.W.Baxter and B.J.Orr, *Rev. Sci. Instrum.*, **70**, 3203 – 3213 (1999).

[9] G.W.Baxter, M.A.Payne, B.D.W.Austin, C.A.Halloway, J.G.Haub, Y.He, A.P.Milce, J.F.Nibler and B.J.Orr, *Appl. Phys. B*, **71**, 651 – 663 (2000) ; see Appendix A.

[10] B.J.Orr, "IR lidar applications in atmospheric monitoring", accepted for publication in *Encyclopedia of Analytical Chemistry: Instrumentation and Applications* (Wiley, 2000).

[11] C.Chang-Hasnain, J.R.Wullert, J.P.Harbison, L.T.Florez, N.G.Stoffel and M.W.Maeda, *Appl. Phys. Lett.*, **58**, 31 (1991); C.Chang-Hasnain, J.P.Harbison, C.-E.Zah, M.W.Maeda, L.T.Florez, N. G.Stoffel and T.-P.Lee, *IEEE J. Quantum Electron.*, **27**, 1368 (1991); C.Chang-Hasnain, M.W. Maeda, J.P.Harbison, L.T.Florez and C.Lin, *J. Lightwave Tech.*, **9**, 1665 (1991); E. Zeeb, B. M_ller, G.Reiner, M.Ries, T.Hackbarth and K.J.Ebeling, *IEEE J. Selected Topics in Quantum Electron.*, **1**, 616 (1995); W.Yuen, G.S.Li and C.Chang-Hasnain, *ibid.*, **3**, 422 (1997); T. Wipiejewski, J.Ko, B.J.Thibeault and L.A.Coldren, *Electron. Lett.*, **32**, 340 (1996).

[12] G.W.Baxter, *PhD Thesis* (Macquarie University, 1998).

[13] E.D.Nelson and M.L.Fredman, *J. Opt. Soc. Am.*, **60**, 1664 – 1668 (1997); M.D.Harwit and N.J.Sloane, *Hadamard Transform Optics*, (Academic Press, London, 1979); M.K.Bellamy, A.N.Mortensen, R.M.Hammaker and W.G.Fateley, *Appl. Spectrosc.*, **51**, 477 – 486 (1997).

[14] M.A.Temsamani and M.Herman, *J. Chem. Phys.*, **102**, 6371 – 6384 (1995).

[15] J.J.Scherer, J.B.Paul, A.O'Keefe and R.J.Saykally, *Chem. Rev.*, **97**, 25 – 51 (1997); J.B.Paul and R.J.Saykally, *Analyt. Chem.*, **69**, 287A – 292A (1997).

[16] K.W.Busch and M.A.Busch (editors), *Cavity-Ringdown Spectroscopy – An Ultratrace-Absorption Measurement Technique* (ACS Symposium Series No. 720; American Chemical Society, Washington, DC, 1999; distributor: Oxford University Press; ISBN 0-8412-3600-3).

[17] Y.He and B.J.Orr, *Chem. Phys. Lett.*, **319**, 131 – 137 (2000).

[18] Y.He and B.J.Orr, "Optical heterodyne signal generation and detection in cavity ringdown spectroscopy based on a rapidly swept cavity," *Chem. Phys. Lett.*, (in press; accepted for publication, 14 December, 2000); see Appendix B.

[19] B.J.Orr and Y.He, "Optical Heterodyne Detection in Cavity Ringdown Spectroscopy," *Australian Provisional Patent Application number PQ9785* filed by Spruson & Ferguson (#521858) for Macquarie University on 30 August 2000.

[20] L.S.Rothman, C.P.Rinsland, A.Goldman, S.T.Massie, D.P.Edwards, J.-M.Flaud, A.Perrin, C. Camy-Peyret, V.Dana, J.-Y.Mandin, J.Schroeder, A.McCann, R.R.Gamache, R.B.Wattson, K. Yoshino, K.V.Chance, K.W.Jucks, L.R.Brown, V.Nemtchinov and P.Varanasi, *J. Quant. Spectrosc. Radiat. Transfer*, **60**, 665 – 710 (1998).

[21] L.S.Rothman, R.L.Hawkins, R.B.Wattson and R.R.Gamache, *J. Quant. Spectrosc. Radiat. Transfer*, **48**, 537 – 566 (1992).

[22] G.Totschnig, D.S.Baer, J.Wang, F.Winter, H.Hofbauer and R.K.Hanson, *Appl. Opt.*, **39**, 2009 – 2016 (2000).

APPENDIX A

G.W.Baxter, M.A.Payne, B.D.W.Austin, C.A.Halloway,
J.G.Haub, Y.He, A.P.Milce, J.F.Nibler and B.J.Orr,
"Spectroscopic diagnostics of chemical processes:
applications of optical parametric oscillators,"
Appl. Phys. B, **71**, 651 – 663 (2000).

(SEPARATELY ATTACHED)

Appl. Phys. B 71, 651–663 (2000) / Digital Object Identifier (DOI) 10.1007/s003400000391

Applied Physics B
Lasers
and Optics

Spectroscopic diagnostics of chemical processes: applications of tunable optical parametric oscillators

G.W. Baxter[1,*], M.A. Payne[1], B.D.W. Austin[1], C.A. Halloway[1], J.G. Haub[1,], Y. He[1], A.P. Milce[1], J.F. Nibler[2], B.J. Orr[1,***]**

[1] Department of Chemistry and Centre for Lasers & Applications, Macquarie University, Sydney, NSW 2109, Australia
(Fax: +61-2/9850-8313, E-mail: brian.orr@mq.edu.au)
[2] Macquarie University Visiting Research Fellow, 1998; permanent address: Chemistry Department, Oregon State University, Corvallis, Oregon 97331-9800, USA
(Fax: +1-541/737-2062, E-mail: niblerj@chem.orst.edu)

Received: 28 March 2000/Published online: 13 September 2000 –

Abstract. Optical parametric oscillator (OPO) and amplifier (OPA) devices are useful for spectroscopic sensing of chemical processes in laboratory, industrial, and environmental settings. This is particularly true of nanosecond-pulsed, continuously tunable OPO/OPA systems, for which we survey a variety of instrumental strategies, together with actual spectroscopic measurements. The relative merits of OPO wavelength control by intracavity gratings and by injection seeding are considered. A major innovation comprises an OPO with a ring cavity based on periodically poled lithium niobate (PPLN) and injection-seeded by a single-mode tunable diode laser (TDL). Active cavity control by an 'intensity dip' method yields an optical bandwidth $\leq 0.005\,\mathrm{cm}^{-1}$ (150 MHz), which compares favourably with the performance of advanced grating-tuned OPO/OPA systems. A novel adaptation of this TDL-seeded PPLN OPO employs a compact, inexpensive multimode pump laser, with which it is still possible to obtain continuously tunable single-mode signal output. Cavity ringdown (CRD) spectroscopy also figures prominently, with infrared (IR) CRD spectra from both grating-scanned and TDL-seeded OPOs reported. Finally, a tunable ultraviolet (UV) source, combining a TDL-seeded passive-cavity OPO and a sum-frequency generation stage, is developed for measurements of time-resolved IR-UV double resonance spectra of acetylene and UV laser-induced fluorescence spectra of nitric oxide.

PACS: 33.20.-t; 42.62.Fi; 42.65.Yj

Over the last thirty years, tunable coherent light sources (lasers and their nonlinear-optical counterparts) have played a vital role in spectroscopic sensing of chemical processes, in industrial or environmental diagnostics and in basic science. One such form of tunable coherent light source, the pulsed optical parametric oscillator (OPO), had an impressive impact in the first of those three decades [1–4], followed by sporadic progress in the second, and a dramatic resurgence of interest and activity within the last ten years [4–8].

This article concentrates on various spectroscopic measurements that have been made recently in our laboratory, using nanosecond-pulsed, continuously tunable OPOs. It surveys OPO-wavelength control strategies that we have found useful for numerous spectroscopic sensing applications [4, 9–20]. The article is neither comprehensive nor retrospective in its outlook. It reports a variety of our significant new experimental results, namely:

- narrowband, single-mode tunability of signal radiation from a compact, low-cost OPO system using a simple multimode Nd:YAG pump laser, an actively controlled ring cavity incorporating periodically poled lithium niobate (PPLN) as the OPO gain medium, and a continuous-wave (cw) single-mode tunable diode laser (TDL) to injection-seed the OPO;
- a TDL-seeded tunable OPO system, based on β-barium borate (BBO), that includes a nonlinear-optical sum-frequency-generation (SFG) stage for laser-induced fluorescence (LIF) spectroscopy and time-resolved optical double resonance (DR) measurements in the ultraviolet (UV) region;
- a first report from our laboratory of OPO-based cavity ringdown (CRD) methods for ultra-sensitive high-resolution molecular absorption spectroscopy in the infrared (IR) region.

Implementation of tunable ns-pulsed OPO light sources entails various spectroscopic detection techniques, appropriate to specific applications. These techniques include:

- optical absorption, both linear and Doppler-free, detected by various means such as LIF, CRD, photoacoustic (PA), and time-resolved IR-UV DR spectroscopy;

*Present address: Physics Department, University of Otago, Dunedin, New Zealand (Fax: +64-3/479-0964; E-mail: gbaxter@physics.otago.ac.nz)
**Present address: Land Operations Division, Defence Science and Technology Organisation, 205L P.O. Box 1500 Salisbury, SA 5108, Australia (Fax: +61-8/8259-5624; E-mail: John.Haub@dsto.defence.gov.au)
***Corresponding author.

- nonlinear-optical techniques such as coherent anti-Stokes Raman spectroscopy (CARS) and degenerate four-wave mixing (DFWM) that are applicable to combustion diagnostics;
- range- and species-resolved atmospheric remote sensing by differential absorption lidar (DIAL).

As a selective example of the mixed success of OPO-based spectroscopic applications over the last thirty years, let us consider the last of the above topics [21,22]. There were a number of impressive early (pre-1982) demonstrations of ns-pulsed, tunable IR OPO systems used for atmospheric remote sensing [23], but then there was a period of ~ 15 years during which relatively few OPO-based advances in IR lidar or DIAL appear to have been made. This is probably because the original tunable ns-pulsed OPOs, almost invariably based on bulk lithium niobate ($LiNbO_3$; abbreviated as LNB), proved difficult to operate and damage-prone (largely because intracavity losses from gratings and étalons caused the operating threshold to approach the damage threshold of optical materials such as LNB). Since then, OPOs have regained acceptance as high-power pulsed tunable sources suitable for spectroscopic applications to atmospheric sensing (for example, by IR DIAL [21,22]). This revival in OPO technology [4–8] is attributable (at least in part) to new nonlinear-optical materials [24] such as BBO and KTP (potassium titanyl phosphate), combined with better pump lasers [25] and advanced injection-seeded OPO system designs [22,26–28].

As already indicated, various instrumental strategies are available to control OPO wavelength for different spectroscopic sensing applications.

At one extreme of operational simplicity are 'free-running' pulsed OPOs, with no intracavity wavelength-selective components, which yield broadband output radiation suitable for low-resolution or multiplex spectroscopy [4, 13, 15]. Such OPOs are based on nonlinear-optical materials [24] that are *either* birefringently phase-matched (BPM) media (using angle- or temperature-tuned bulk media such as LNB, BBO, or KTP) *or* quasi-phase-matched (QPM). QPM media, such as PPLN [29,30], offer higher nonlinear-optical coefficients, lower operating thresholds, and smaller size than BPM OPO materials.

At the other extreme of operational complexity are narrowband continuously tunable ns-pulsed OPOs that have been used for a variety of high-resolution spectroscopic applications, typically with single-mode signal or idler output radiation of narrow optical bandwidth. Such narrowband tunable OPOs may be controlled by intracavity gratings or étalons [3–7,31–37]. Within the last decade, a popular alternative approach to narrowband ns-pulsed OPO tuning has been injection seeding with a dye laser [4,5,9–12,38], a single-mode TDL [14–20,26–28,39–44], or other forms of tunable coherent source [44–47]. Earlier work on injection-seeded OPOs has been reviewed [4,10].

Another useful approach to wavelength control of pulsed OPOs employs 'spectroscopic tailoring' to generate structured, multi-wavelength output radiation that has potential for further advances in multiplex spectroscopy [9,10,22,48]. Other aspects include nonlinear-optical wavelength extension [24] of tunable, ns-pulsed OPO output into the visible or UV regions by sum-frequency generation (SFG) [4,11, 49–51] or into the IR via an optical parametric amplifier (OPA) stage [12,13,52] or by difference-frequency generation (DFG) [2,24,46]. There are also many significant advances [8] in continuous-wave tunable OPO and DFG systems, pumped by cw-TDLs and other forms of cw solid-state laser, and in ultra-fast (ps, fs) pulsed OPOs but these lie outside the scope of this already-wide-ranging article.

The versatility and flexibility in design is largely attributable to the fact that an OPO is a nonlinear-optical device, not a laser. This facilitates methods of temporal and wavelength control (and, consequently, appropriate spectroscopic detection schemes) that are not possible with lasers. The latter generally depend on population inversion of an optical gain medium, with associated optical lifetime and saturation limitations. On the other hand, optical parametric gain, oscillation and amplification are more amenable to modular system design because they depend on nonlinear-optical coefficients and phase-matching conditions.

The OPO-based technological and scientific developments that have evolved in our laboratory over the last decade have been influenced by constructive interactions with a number of research groups in Germany, including those of Wallenstein (Kaiserslautern) [9,10], Huisken (Göttingen), and Andresen (Göttingen and Bielefeld). Our regular contact with the Wolfrum group in Heidelberg has been particularly helpful, by providing much stimulation, relevance and challenge for our own research programme. It is therefore fitting for this article to pay tribute to Professor Dr Jürgen Wolfrum, for his impressive range of achievements in both pure and applied science and for the personal drive and vision characterising the research that he and his colleagues pursue.

1 Instrumentation: OPO-wavelength control

Optical parametric oscillators typically involve coherent three-wave nonlinear-optical processes in non-centrosymmetric solid-state media [1–7,24], in which a single laser input wave ('pump', frequency ω_P) and two coherent output waves ('signal', frequency ω_S; 'idler', frequency ω_I; $\omega_S \geq \omega_I$) obey both energy conservation and phase-matching conditions:

$$\omega_P = \omega_S + \omega_I \; ; \; \boldsymbol{k}_P - \boldsymbol{k}_S - \boldsymbol{k}_I - \Delta\boldsymbol{k} = 0 \, . \qquad (1)$$

Here $\boldsymbol{k}_j$ is a wave vector (with magnitude $k_j = n_j\omega_j/c = 2\pi n_j/\lambda_j$, where n_j is the refractive index at vacuum wavelength λ_j and c is the speed of light; j = P, S, or I) and $\Delta\boldsymbol{k}$ is a phase-mismatch increment that must be minimised to optimise OPO conversion efficiency and thereby control the output signal and idler wavelengths, λ_S and λ_I. Traditionally, this is done by adjusting the angle and/or temperature of a birefringent nonlinear-optical crystal via its ordinary- and extraordinary-ray refractive indices [24]. A recently implemented alternative is to use QPM media tailored for specific wavelengths by periodic optical structuring, with PPLN as a prominent example [19,20,29,30].

The OPO-based spectroscopic systems of interest here are typically pumped by high-performance ns-pulsed solid-state lasers [25]. Our standard OPO pump laser is a 1.064-μm flashlamp-pumped, Q-switched Nd:YAG oscillator/amplifier system (Spectra-Physics GCR-5 or GCR-250), equipped with an injection seeder for single-longitudinal-mode (SLM) operation [25], special cavity optics to yield a quasi-Gaussian

beam profile, and nonlinear-optical stages to generate harmonics at 532 nm and 355 nm. Typical operating parameters include: pulse duration, ~ 8 ns; repetition rate, 10 Hz; pulse energies, ≥ 1 J at 1.064 μm, ≥ 0.7 J at 532 nm, ≥ 400 mJ at 355 nm. With a confocal Fabry–Pérot étalon, we have measured the optical bandwidth of one such SLM pulsed laser to be 45 ± 5 MHz ($0.0015 \pm 0.0002\,cm^{-1}$) FWHM, via a convolution of Gaussian (~ 35 MHz) and Lorentzian (~ 10 MHz) components [20].

It is also possible to employ a less elaborate multimode (MM) pump laser and still attain single-mode tunability of OPO signal or idler radiation, as will be demonstrated in Sects. 1.4 and 2.2. The simple, compact MM Nd:YAG laser employed here (Continuum Minilite II) delivers ~ 50 mJ/pulse at 1.064 μm and repetition rate of 10 Hz. It oscillates on several longitudinal modes, yielding an optical bandwidth of ~ 1 cm^{-1} and a rapidly modulated temporal profile (~ 6 ns FWHM). It uses regular mains power and is air-cooled, thereby facilitating field-based OPO applications.

OPO pumping by all-solid-state (for example, diode-pumped) ns-pulsed lasers is an increasingly attractive option [36, 37, 53–56] offering high repetition rates (≥ 1 kHz) and portability.

Another constructive approach is to use an optical parametric generator (OPG) or amplifier (OPA), rather than an OPO, thereby eliminating the need to enclose the nonlinear-optical gain medium in an optical cavity. An early realisation used a KTP OPA for DFG-type mixing of dye-laser and 532-nm Nd:YAG radiation for degenerate four-wave mixing (DFWM) IR spectroscopy of jet-cooled acetylene (C_2H_2) [57]. More recently, this approach has been facilitated by high-gain QPM media, such as PPLN, pumped by high-repetition-rate all-solid-state ns-pulsed lasers, as in the following two instances: a PPLN OPA seeded by an étalon-filtered PPLN OPG with an idler bandwidth of ≤ 0.08 cm^{-1} has been used to record spectra of CH_4 gas by long-path absorption and degenerate four-wave mixing (DFWM) [58]; a ns-pulsed PPLN OPG has yielded high signal-conversion efficiency (23% maximum) and been spectrally narrowed by seeding with a He-Ne laser [59].

1.1 Free-running BPM OPOs

One of the most primitive forms of ns-pulsed OPO uses a suitable nonlinear-optical crystal (typically BPM using either angle- or temperature-tuning) in a two-mirror optical cavity that is resonant at either λ_S or λ_I. It is pumped at λ_P by a pulsed monochromatic coherent source (for example, harmonics of a Nd:YAG laser). Numerous high-quality bulk OPO materials (such as LNB, BBO and KTP) are now commercially available, with different cuts of OPO crystal needed for different spectral regions [24].

When a BPM OPO operates in a free-running mode (i.e., with no wavelength-selective elements), its output radiation has a broad optical bandwidth (typically ~ 10 cm^{-1} or more), depending on several factors [1–7, 13, 15, 60–64]: the refractivity, dispersion, and absorption of the OPO medium; the wavelengths λ_S, λ_I, and λ_P; the type of phase matching (and whether it is collinear or not); the crystal dimensions; the cavity reflectivity and effective number of passes of the resonated wave; the optical bandwidth, divergence, pulse duration and pulse energy of the pump radiation.

1.2 Free-running QPM OPOs

Pulsed, free-running OPOs based on QPM nonlinear-optical media can employ a two-mirror optical cavity (resonant at either λ_S or λ_I) virtually as simple as those for bulk BPM media (as in Sect. 1.1). QPM devices offer higher nonlinear-optical coefficients and smaller size than BPM materials. For instance, in our previous work [19, 20] and ongoing research (see Sect. 1.4), we use a commercially available PPLN element (Crystal Technologies Inc.) that is 19 mm long × 11 mm broad × 0.5 mm thick with a set of eight parallel QPM gratings of varying periodicity (28.5–29.9 μm, in 0.2-μm steps) on a single substrate. At a fixed OPO crystal temperature, a single PPLN grating generates broadband signal and idler output spread over ~ 5 cm^{-1} (~ 150 GHz) FWHM. With 1.064-μm pump radiation, this combination of eight PPLN grating periods and temperature variation over ~ 50 °C provides uninterrupted QPM OPO tuning ranges of 1.45–1.55 μm for the signal and 4.0–3.4 μm for the idler.

There is much current interest in free-running ns-pulsed QPM OPOs [53–56, 65], particularly with novel solid-state pump lasers or with new periodically poled (PP) materials, such as PPKTP and PPRTA (rubidium titanyl arsenate), that are now available to supplement PPLN. However, for many spectroscopic purposes it is necessary to use additional ways to narrow the optical bandwidth and control the output wavelengths.

1.3 Grating-tuned OPOs

As indicated above, the conventional way to achieve narrowband operation of a ns-pulsed OPO is by means of wavelength-selective elements, such as intracavity gratings and/or étalons. This was realised by Byer and colleagues in early ns-pulsed LNB OPOs [3, 4, 23] and subsequently further developed in other BPM OPOs [31–34]. For instance, the advanced Bosenberg–Guyer design of a KTP OPO/OPA system [32] provides a practical narrowband pulsed spectroscopic source, continuously tunable under computer control over wide IR ranges (1.3–4 μm) with narrow optical bandwidth. Such an instrument is commercially available in the form of the Mirage 3000 OPO/OPA system (STI Optronics/Continuum), with a specified optical bandwidth of ≤ 500 MHz (≤ 0.017 cm^{-1}). There are prime examples of this spectroscopic system's utility for IR degenerate four-wave mixing (DFWM) [66, 67] and CRD [68] studies of molecules and combustion media. Careful operation of such a system yields 3.5-ns IR pulses with an effective scanning bandwidth of < 0.007 cm^{-1}, compared to a single-shot bandwidth of ~ 0.004 cm^{-1} [67, 68]. Our Continuum Mirage 3000 system, used to obtain results reported in Sects. 2.2 and 2.3 below, is pumped by a SLM Nd:YAG laser (Continuum 8000) delivering ~ 7-ns pulses with a repetition rate of 10 Hz at 532 nm (~ 20 mJ into the master oscillator; ~ 90 mJ into the non-resonant oscillator) and 1.064 μm (~ 330 mJ into the OPA stage); it thereby generates narrowband tunable IR output at 0.5–10 mJ per signal or idler pulse, depending on output wavelength.

Narrowband tunable ns-pulsed QPM OPO systems (for example, those based on PPLN) can also be controlled by intracavity gratings or étalons [35–37]. However, our preferred

alternative is to employ injection-seeded PPLN OPOs, as described in the next section.

1.4 Injection-seeded OPOs: actively controlled cavities

Injection seeding is a particularly successful approach to controlling the wavelengths and optical bandwidth of a ns-pulsed OPO [4, 5, 9–12, 14–20, 26–28, 38–48]. This simplifies OPO construction, with a narrowband, low-power external source of tunable radiation separating the OPO's wavelength-control function from that of power amplification.

The prime objective is to tune the signal and idler output wavelengths of the injection-seeded ns-pulsed OPO without mode hopping as the seed laser wavelength is scanned. One way to achieve this is by progressively varying instrumental settings, such as OPO crystal angle, by means of a computer-controlled "look-up table". Such an approach has been successfully adopted in previous injection-seeded OPO systems [42, 46]. For instance, the injection-seeded tunable OPO system of Huisken and colleagues [46] comprises a 1.064-μm pumped LNB OPO seeded at its idler wavelength by a DFG stage that mixes 532-nm Nd:YAG and tunable visible dye laser radiation; continuous tuning over ranges of at least 50 cm^{-1} is achieved by computer control of the phase-matching angles of all of the nonlinear-optical crystals as the dye-laser diffraction grating is rotated. This DFG-seeded LNB OPO system has been used [69] to measure DFWM and stimulated Raman scattering (SRS) spectra of C_2H_2, carbon dioxide (CO_2) and nitrous oxide (N_2O), in gases and free jets.

For more demanding spectroscopic applications, requiring narrowest-possible optical bandwidth and high spatial beam quality, active control of the injection-seeded OPO cavity length is generally necessary for stable, continuously tunable SLM operation. This is best achieved by actively varying the OPO cavity length synchronously with the wavelength scan of the seed source, using some form of optoelectronic feedback to stabilise the process. Progress on this front so far has been limited, with only a few published reports of high-resolution spectra actually recorded by actively tuning output radiation from an injection-seeded ns-pulsed OPO (either continuously [19, 20, 38, 40] or in fine wavelength steps [26]).

We have recently reported a modular high-performance spectroscopic system comprising a TDL-seeded PPLN OPO with an actively controlled ring cavity, *plus* a bulk-LNB OPA stage for some applications [19, 20]. That modular PPLN OPO/OPA system is pumped at 1.064 μm by a SLM ns-pulsed Nd:YAG laser, injection-seeded by a cw TDL at ~ 1.5 μm, and generates coherent narrowband IR signal and idler outputs that are continuously tunable in the vicinities of ~ 1.5 μm and ~ 3.5 μm, respectively. We use a novel intensity-dip control scheme to lock the length of the OPO ring cavity to the single-mode TDL seed radiation. Our spectroscopic experiments with output from this ns-pulsed PPLN OPO demonstrate a remarkably narrow effective scanning bandwidth of 135 MHz (0.0045 cm^{-1}) and good beam quality. This offers prospects for high-resolution, time-resolved laser spectroscopy, particularly in molecular-beam environments or in gases at low pressure.

We now report a less expensive, more compact variant of the above PPLN OPO design which still provides narrowband, single-mode tunability of its signal output radiation. It incorporates the same form of actively controlled, TDL-seeded ring cavity as above [19, 20] but is pumped by multimode 1.064-μm radiation from the much less sophisticated ns-pulsed MM Nd:YAG laser described in the preliminary part of Sect. 1. A schematic of this new MM-pumped PPLN OPO system is presented in Fig. 1.

With this less elaborate PPLN OPO design, we find that it is possible to employ a *multimode* (MM) pump laser and still attain *single-mode* tunability of OPO signal or idler radiation. Our MM-pumped PPLN OPO uses the resonance properties of the OPO ring cavity to constrain the resonated wave (the signal is resonant in this instance) to a single longitudinal cavity mode and to ensure that it is continuously tunable without mode hops as the cavity length and TDL-seed wavelength are scanned. When the cavity is in resonance with the cw seed radiation, the total intensity of that radiation reflected off the cavity displays a pronounced dip; as before [19, 20], this intensity dip serves as a locking signal to reset the cavity length piezoelectrically during each interval between pump-laser pulses.

The coherent infrared signal output from this TDL-seeded, MM-pumped PPLN OPO has a narrow optical bandwidth (~ 135 MHz, ~ 0.0045 cm^{-1}) and beam quality comparable to those of our previous TDL-seeded PPLN OPO [19, 20] pumped by a single-mode Nd:YAG laser. A single PPLN grating (on a multi-grating substrate [30]; described in Sect. 1.2 above) allows continuous tunability over the following ranges in the 1.5-μm region: ~ 400 GHz (~ 13 cm^{-1}) at constant temperature; ~ 7.5 THz (~ 250 cm^{-1}) with additional temperature tuning. This performance has been verified by Fabry–Pérot étalon and grating spectrometer measurements, and by recording actual high-resolution molecular spectra, some of them below the Doppler limit (as discussed in Sect. 2.2 below). The idler output remains multi-

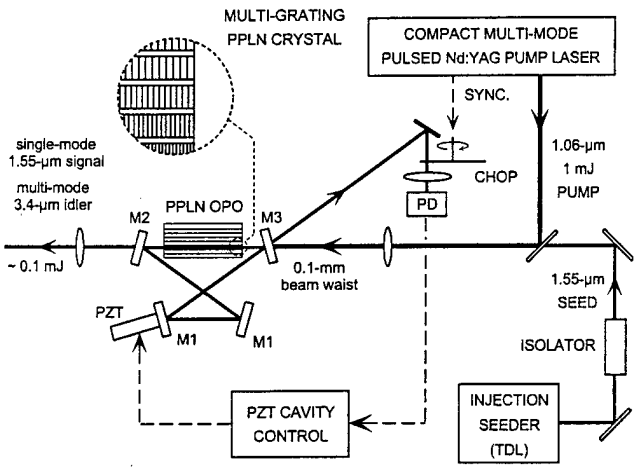

Fig. 1. Modular schematic of a narrowband, tunable PPLN OPO spectroscopic system, pumped at 1.064 μm by a ns-pulsed, multi-mode (MM) Nd:YAG laser. The actively controlled PPLN OPO ring cavity is injection-seeded at its (resonant) signal wavelength of ~ 1.55 μm by a 5-mW cw single-mode external-cavity diode laser (TDL). The output of the multi-grating PPLN crystal (see *inset*) can be coarsely tuned by vertical positioning and/or temperature variation. Despite using a MM pump laser, active OPO cavity control ensures that the 1.55-μm OPO signal output is single-mode; the corresponding 3.4-μm idler output is multi-mode. Not shown in this schematic are optional extra KTP SFG and LNB OPA stages for optical diagnostics and amplification, respectively. See text for further details

mode, consistent with the characteristics of the MM pump laser. With a typical 1.064-μm MM pump laser energy of ~ 1 mJ/pulse (approximately twice the free-running PPLN OPO operating threshold), we obtain a total output energy (SLM signal + MM idler) of ~ 0.1 mJ/pulse.

More details of the MM-pumped PPLN OPO system shown in Fig. 1 will be presented elsewhere [70], together with full operating characteristics and further spectroscopic results.

1.5 Injection-seeded OPOs: passive misaligned cavities

An alternative approach to injection-seeded tuning, which has been used extensively by our group in the context of ns-pulsed BPM OPOs based on BBO [4, 9–12, 14–17] and LNB [18], entails passive control of the OPO cavity by slightly misaligning one of its reflectors. This facilitates continuous tuning of the injection-seeded OPO signal and idler outputs by decreasing the effective finesse of the OPO cavity, so that it is not necessary to lock the OPO cavity length to the seed wavelength, and is therefore simpler optically and electronically than active control of the OPO cavity. The method depends on the OPO cavity having a high Fresnel number, so that a series of high-order transverse modes can smooth out the sharp, widely separated resonances that occur when the OPO cavity is well aligned; a resulting disadvantage is that the multiple transverse modes tend to cause some degradation of output beam quality. Nevertheless, this passive-cavity approach has proved useful for many applications of tunable OPOs, with seeding by either pulsed dye-lasers [9–12] or single-mode TDLs [14–17]; this is further demonstrated in Sects. 2.1 and 2.4 below.

This passive, misaligned-cavity technique facilitates injection seeding of ns-pulsed BPM OPOs via spatial and spectral properties of nonlinear-optical processes that are now reasonably well established, on the basis of investigations in our own laboratory [13, 15, 17, 71–73] and elsewhere [47, 63, 64, 74].

A series of experiments [72] has been performed to elucidate the spatial and spectral properties of free-running and injection-seeded BBO and LNB OPOs, with various degrees of cavity misalignment. Periodic variations in OPO output intensity are observed as either cavity length or seed wavelength are scanned; the relative depth of this periodic modulation is markedly reduced as a cavity reflector is slightly misaligned in steps of ~ 0.5 mrad. These correlate with the optical transmission characteristics of the unpumped OPO cavity at both signal and idler wavelengths and are satisfactorily explained in terms of cavity resonance properties. Single-shot OPO beam imaging techniques have also been used [72] to examine signal output beam profiles and spectro-spatial distributions for BBO and LNB OPOs, both TDL-seeded and free-running. Details will be presented in forthcoming publications [73].

Other spatio-spectral effects have been observed in BBO and KTP OPOs [13, 15] and exploited in a simple free-running BBO OPO for DFWM spectroscopy of sodium atoms in a flame, by spatially filtering the beam and scanning the phase-matching angle [15].

1.6 OPO wavelength extension: SFG, DFG and OPA

Coherent nonlinear-optical wavelength conversion is intrinsic to OPO-based spectroscopic sensing, not only in the primary OPO (or OPA or OPG) process itself but also in various harmonic-, sum- and difference-frequency generation processes that are implicated in the pump laser itself or in subsequent wavelength-conversion stages. It is not our intention to survey this vast topic [24], but rather to point out how nonlinear-optical wavelength conversion enhances the versatility and utility of OPO-based spectroscopic systems.

We have already alluded in the introduction to sum-frequency generation (SFG) [4, 11, 49–51] as a means of extending OPO output wavelengths to shorter wavelengths, notably in the UV region. In particular, we note the enhanced OPO SFG conversion efficiency achieved by Fix and Ehret [51] with intracavity mixing media: at least a twofold increase in UV output energy relative to conventional external OPO SFG [4, 11, 49, 50].

A new OPO/SFG apparatus for various UV-spectroscopic applications (see Sects. 2.3 and 2.4 below) is depicted in Fig. 2. It comprises a ring-cavity BBO OPO, pumped at wavelength λ_P (typically 355 nm) by output from a high-power SLM Nd:YAG laser, injection seeded at λ_I (typically ~ 1.5 or 0.82 μm from a single-mode external-cavity TDL), and operated in the passive, misaligned cavity mode outlined in Sect. 1.5. The OPO signal or idler output (at λ_S or λ_I, respectively) is combined collinearly with a laser beam at λ_L (typically 1.064 μm or 355 nm) then both beams are reduced by a 2.5:1 telescope and coherently mixed to generate the desired tunable UV output at λ_{SFG}. Three versions of this apparatus are summarised in Table 1, together with key performance characteristics. The SFG conversion efficiencies so far attained by this method are unremarkable, although the resulting pulse energies (1–3 mJ) are ample for significant UV-spectroscopic applications, as shown in Sects. 2.3 and 2.4 below.

Another useful role for SFG in OPO applications is up-converting IR OPO output in wavelength regions where commonly available wavemeters and beam-imaging instruments are unresponsive. For instance, this approach is used exten-

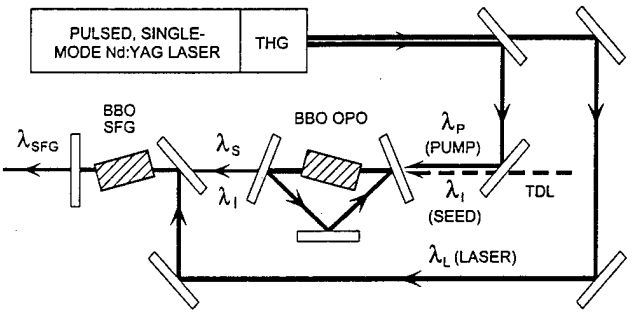

Fig. 2. Modular schematic of a narrowband, tunable BBO OPO/SFG UV-spectroscopic system, pumped at 355 nm by the third-harmonic output (355 nm) of a ns-pulsed single-mode Nd:YAG laser. The OPO comprises a birefringently phase-matched (BPM) BBO crystal in a passive ring cavity that is injection-seeded at the (non-resonant) idler wavelength λ_I by radiation from a cw single-mode TDL. The UV SFG output at λ_{SFG} is generated in a second BPM BBO crystal by coherent mixing of OPO signal or idler radiation (λ_S or λ_I) with one of the Nd:YAG laser harmonics (λ_L). See text and Table 1 for further details

Table 1. Design parameters for the OPO/SFG system depicted in Fig. 2, specifying applications and modes of operation for three key UV output wavelength regions

Application (and mode of operation)	C_2H_2 IR-UV DR (see Sect. 2.3)	NO 0-0 band (see Sect. 2.4)	NO 0-2 band (see Sect. 2.4)
UV output λ_{SFG}/nm	~ 323[a]	~ 226[a]	~ 247[a]
UV output pulse energy /mJ	2–3	1–2	2–3
UV output pulse width /ns	~ 3	~ 4	~ 3
TDL seed λ_I/nm	~ 1510[b]	~ 824[b]	~ 814[b]
TDL seed power /mW	~ 2	~ 5	~ 5
OPO pump λ_P/nm	355[a]	355[a]	355[a]
Pump pulse energy /mJ	~ 210	~ 180[c]	~ 180[c]
OPO crystal (@ cut angle)[d]	BBO (@ 30°)	BBO (@ 30°)	BBO (@ 30°)
SFG crystal (@ cut angle)[d]	BBO (@ 30°)	BBO (@ 53°)	BBO (@ 53°)
OPO output used for	$\lambda_S \approx 463$ nm	$\lambda_S \approx 623$ nm	$\lambda_I \approx 814$ nm
SFG (@ pulse energy)	(@ ~ 10 mJ)[b]	(@ ~ 10 mJ)[b]	(@ ~ 10 mJ)[b]
Laser output used for	$\lambda_L = 1064$ nm	$\lambda_L = 355$ nm	$\lambda_L = 355$ nm
SFG (@ pulse energy)	(@ ~ 190 mJ)[b,e]	(@ ~ 30 mJ)[b,c]	(@ ~ 30 mJ)[b,c]

[a] Horizontally polarised
[b] Vertically polarised
[c] The ratio of vertically polarised $\lambda_L = 355$-nm SFG laser radiation to horizontally polarised $\lambda_P = 355$-nm OPO pump radiation is optimally controlled by adjusting a polarising beam-splitter; the SFG laser input is synchronised with the OPO output by an optical delay
[d] Each BBO crystal is Type-I birefringently phase-matched, with a horizontal phase-matching plane
[e] The 1064-nm laser radiation is low-quality residual output from the THG stage of the Nd:YAG laser; it is passed through a linear polariser and optical delay line but is still poorly matched (spatially and temporally) to the OPO output, so that the SFG efficiency is low

sively for OPO beam diagnostics in our studies of narrowband LNB and PPLN OPOs [18–20]. This optical diagnostic technique relies on having a well-characterised pulsed laser beam (for example, a small portion of the 1.064-μm fundamental radiation from a high-performance SLM Nd:YAG laser, as specified in the preliminary part of Sect. 1) to use for reference purposes. A KTP nonlinear-optical SFG crystal ($\theta = 51°$, $\varphi = 0°$, type-I phase-matched [24]) is then used to mix this 1.064-μm laser radiation with the 1.5-μm signal beam from the TDL-seeded LNB or PPLN OPO [18–20], generating SFG output at ~ 620 nm for diagnostics of optical beam quality and spectral purity by a fixed étalon as well as accurate wavelength calibration by a pulsed wavemeter (Burleigh WA-4500). A similar approach has been used to characterise the performance of the new MM-pumped PPLN OPO to which Sects. 1.4 and 2.2 refer; the (high-power) SLM Nd:YAG laser pulses are then synchronised with the OPO output pulses from the (low-power) MM Nd:YAG laser.

For applications requiring 3.4-μm idler radiation or higher 1.55-μm signal-wave power, the horizontally polarised beam from our TDL-seeded PPLN OPO (either SLM-pumped [19, 20] or MM-pumped, as in Sects. 1.4 and 2.2) is coupled into an OPA stage, pumped at 1.064 μm by a high-power SLM laser (vertically polarised, typically 200 mJ/pulse; the OPO pump laser can double in this role if it is SLM). This OPA unit comprises a BPM LNB crystal ($11 \times 11 \times 50$ mm, 47°-cut for type-I phase matching in the vertical plane [24], broadband anti-reflection coated) identical to that in our previously reported TDL-seeded LNB OPO [18]. In either case, it is necessary to synchronise the high-power SLM Nd:YAG laser pulses with the PPLN OPO signal output pulses for optimum OPA conversion efficiency.

In this general context, mention should also be made of coherent difference-frequency generation (DFG) [2, 24]. In nonlinear-optical terms, this corresponds closely to OPA and injection-seeded OPG processes, the essential distinction arising from the relative magnitudes of the input radiation fields involved. That is, the two input fields are generally of comparable amplitude in the case of DFG, whereas the pump field is usually much stronger than the other (signal, idler, or seed) field in the OPA or seeded OPG cases. Relative to DFG, the added complexity of cavity control in an OPO may be offset by the higher output power and coherence that is advantageous in many spectroscopic sensing applications.

2 Spectroscopic applications of ns-pulsed OPOs

Spectroscopic measurements play a central role in our programme of OPO-related research. Such measurements are not only of interest *per se*, in the context of spectroscopic sensing of molecular processes and industrial or environmental media, but they are also able to provide realistic performance tests for the tunable OPOs developed. This duality is evident in our previous publications [4, 9–20] and also in the fresh examples that follow.

2.1 Photoacoustic absorption spectroscopy

Photoacoustic absorption (PA) spectroscopy provides a straightforward way to record Doppler-limited spectra of molecules in gases. This method has featured prominently in much of our developmental work on injection-seeded ns-pulsed OPOs (BBO, LNB, and PPLN) [4, 9–11, 14, 15, 18, 19], as a convenient way to demonstrate that the OPO output is continuously tunable without mode hops or abrupt optical power fluctuations. A typical experimental setup is depicted in Fig. 3, with an OPO based on BPM BBO in a passive, slightly misaligned ring cavity pumped by a SLM Nd:YAG laser and injection-seeded by a 1.5-μm external-cavity TDL. PA signals arising from absorption of the gas-phase molecules are detected by a small electret microphone located near the midpoint of the long axis of a cylindrical sample cell.

Figure 4a presents a high-resolution OPO PA spectrum of ammonia (NH_3) gas (temperature $T = 300$ K, pressure

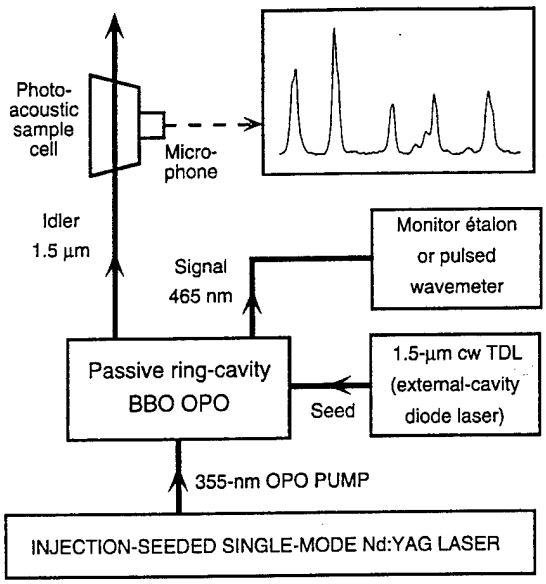

Fig. 3. Schematic of an OPO-based spectroscopic system for high-resolution pulsed photoacoustic absorption (PA) spectroscopy. Horizontally polarised third-harmonic output (355 nm) of a ns-pulsed single-mode Nd:YAG laser is used to pump the OPO, which comprises BBO in a passive ring cavity that is injection-seeded at the (non-resonant) idler wavelength (~ 1.5 μm) by vertically polarised radiation from a cw single-mode TDL. The vertically polarised IR OPO idler output is passed through an optical absorption cell to record PA spectra, while the visible signal output is sent to an étalon to monitor the seeding process

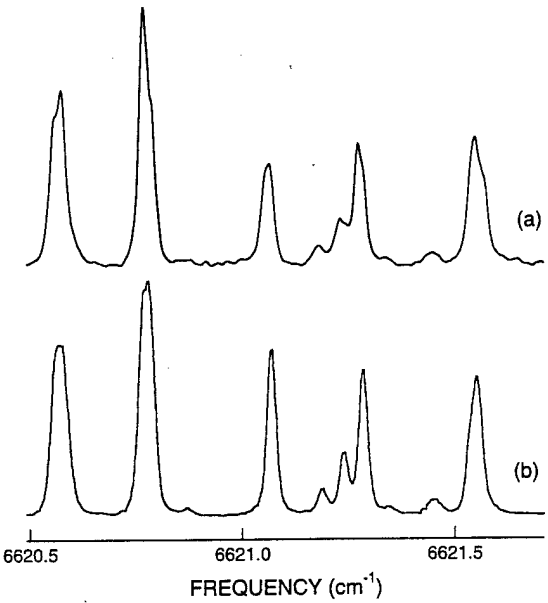

Fig. 4. IR absorption spectra of a portion of the ($\nu_2 + \nu_3$) rovibrational combination band of ammonia gas, NH_3. Trace (a) is a photoacoustic absorption spectrum for 5-Torr NH_3, recorded using ~ 5 mJ/pulse of 1.51-μm idler output from a passive ring-cavity injection-seeded BBO OPO. Trace (b) is a reference absorption spectrum for 9.5-Torr NH_3 recorded with a high-resolution FTIR spectrophotometer [75]

$P = 5$ Torr) using idler radiation at ~ 1.51 μm from the pulsed, TDL-seeded BBO OPO. This spectrum is recorded in a continuous scan of the idler wavelength, without correcting for any shot-to-shot variations of IR pulse energy. The region recorded is part of the ($\nu_2 + \nu_3$) rovibrational combination band of NH_3, for which a closely corresponding high-resolution ($\sim 0.005\,cm^{-1}$) Fourier-transform infrared (FTIR) spectrum of NH_3 at 9.5 Torr is shown in Fig. 4b [75]. The FWHM widths of unblended lines in Fig. 4a and b are $\sim 0.028\,cm^{-1}$ and $0.022\,cm^{-1}$, respectively; allowing for Doppler broadening ($0.02\,cm^{-1}$) and pressure broadening (~ 40 MHz Torr^{-1} [75]), we deduce an effective spectroscopic bandwidth of $< 0.02\,cm^{-1}$ (< 600 MHz) for the continuously scanned OPO idler radiation.

Spectra such as that in Fig. 4a and elsewhere [4, 14, 15, 18] confirm that the ns-pulsed signal or idler output of a TDL-seeded BPM OPO with a passive, slightly misaligned ring cavity can indeed be continuously scanned with a high degree of pulse-to-pulse stability. Moreover, such PA spectroscopic measurements are evidently insensitive to spatial variations now known [72, 73] to exist on the OPO output beam profiles (as discussed in Sect. 1.5 above). To obtain spectra of this quality, it is therefore not necessary to lock the OPO cavity length to the seed laser wavelength.

Other instances of PA spectroscopy arise in Sects. 2.2 and 2.3 below, where the method proves useful for IR wavelength calibration and spectroscopic assignment.

2.2 High-resolution OPO CRD spectroscopy

Cavity ringdown (CRD) spectroscopy is a sensitive, accurate way to acquire weak optical absorption spectra [76]. The technique entails recording the energy loss rate of an absorbing optical medium when monochromatic light (usually ns-pulsed) is multiply reflected within a high-finesse optical cavity containing the medium of interest. High-reflectivity cavity mirrors yield typical ringdown times of a few μs, yielding a very long effective absorption path length. Moreover, the ringdown time is usually independent of light intensity, so that sensitivity is not limited by optical intensity fluctuations, as prevails in most forms of laser spectroscopy. These two features together account for the high sensitivity of CRD spectroscopy.

We have recently reported a novel form of CRD spectroscopy, using a cw TDL and a rapidly-swept ringdown cavity [77]. However, in the present paper we consider the more traditional, simpler form of CRD spectroscopy using ns-pulsed lasers or OPOs. We focus here on IR CRD spectroscopy with various forms of pulsed, tunable OPO operating in the ~ 1.55 μm wavelength region. Earlier OPO- or OPA-based IR CRD spectroscopy has already been cited [57, 68, 69], so that the novelty of the results that we now report lies more in our OPO instrumentation and technique than in the CRD spectra themselves.

This emphasis on innovative instrumentation is evident in the first of the two examples of OPO CRD spectroscopy that we present. It entails using the MM-pumped, TDL-seeded PPLN OPO system described in Sect. 1.4 above to record high-resolution CRD spectra of CO_2 gas ($T = 300$ K, $P = 1$ bar) in the 1.54-μm near-IR region, as shown in the upper portion of Fig. 5. The full spectrum was recorded in a single 120-cm^{-1} sweep over a period of ~ 1 h and is faithfully reproduced by the adjoining simulated spectrum derived from the HITRAN'96 database [78]. The CRD spectrum is seen to arise from the weak 6503-cm^{-1} 30^01–00^00 rovibrational combination band of CO_2 and the nearby (even weaker)

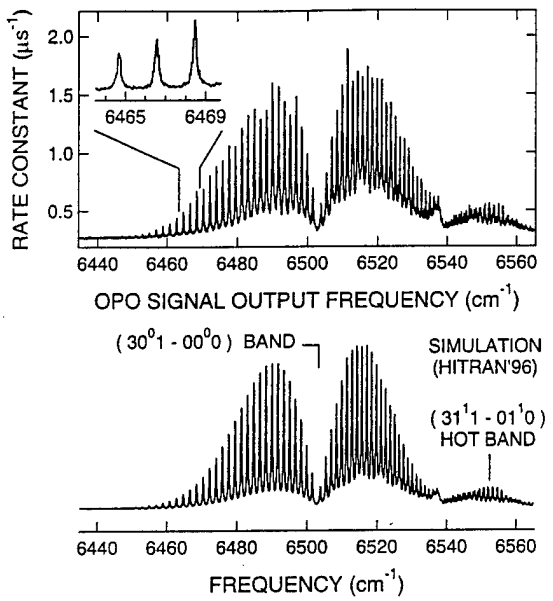

Fig. 5. Rovibrational IR absorption spectra of combination and hot bands at $\sim 6500\,cm^{-1}$ (1.54 μm) for CO_2 gas ($T = 300$ K; $P = 1$ bar). The *upper portion* shows CRD spectra (including an inset enlargement of the region between 6464 cm^{-1} and 6469 cm^{-1}) recorded by continuously scanning the signal output wavelength of a MM-pumped, TDL-seeded PPLN OPO system (see Sect. 1.4 and Fig. 1). The lower portion shows a simulation derived from the HITRAN'96 database [78]. See text for a detailed discussion of CRD lineshape effects

6536-cm^{-1} 31^11–01^10 hot band [78, 79]. The three rovibrational features at 6464–6469 cm^{-1} shown in the insert are the P(39), P(41) and P(43) lines of the main band; they are baseline-resolved with pressure-broadened linewidths of $\sim 0.2\,cm^{-1}$. The observed noise level corresponds to an absorbance detection sensitivity of $7 \times 10^{-8}\,cm^{-1}$.

The best-fit HITRAN simulation of the CRD spectra in Fig. 5 assumes that the MM-pumped, TDL-seeded PPLN OPO radiation comprises two equally weighted components of pulse energy: an intense narrowband Gaussian spike (0.005 cm^{-1} FWHM) on a broadband Lorentzian 'pedestal' (0.35 cm^{-1} FWHM) that is much less intense (< 1% in terms of spectral irradiance). Other CRD spectra of CO_2 (not presented here) have been recorded in a similar spectral region but at a much lower pressure (0.6 Torr); the measured FWHM linewidth of 0.015 cm^{-1} (450 MHz) then corresponds to the Doppler profile (0.012 cm^{-1} FWHM) convoluted with an OPO effective scanning bandwidth of $\sim 0.009\,cm^{-1}$ (270 MHz).

The apparatus used to obtain the OPO CRD spectra shown in Fig. 5 comprises the MM-pumped, TDL-seeded PPLN OPO system (see Sect. 1.4 and Fig. 1) and an evacuable sample chamber housing the ringdown cavity, followed by a fast InGaAs photodiode with preamplifier (50-MHz bandwidth) and a 200-MHz digital oscilloscope (Tektronix TDS350). The ringdown cavity itself comprises two highly reflective (> 99.96%) concave mirrors (Newport 10CV00SR.70F) with a curvature of −1 m, separated by 0.17 m and carefully aligned. This yields an empty-chamber ringdown time of 3.8 μs, which diminishes appreciably when the IR radiation is scanned through an absorption feature in the spectrum of interest. The preamplified photodetector output voltage provides a CRD waveform that is averaged in the digital oscilloscope for successive optical pulses from the OPO (at a repetition rate of 10 Hz). The averaged data are computer-analysed by means of an algorithm that estimates the ringdown time by fitting a single-exponential function to the decay curve and using the inverse of the exponential decay time to plot the CRD spectrum. This combination of MM-pumped, TDL-seeded PPLN OPO system together with associated CRD instrumentation results in a spectroscopic system that is considerably more compact and less expensive than traditional CRD apparatus based on large-frame ns-pulsed Nd:YAG lasers pumping a dye laser or OPO/OPA system [68, 69, 76]. More instrumental details and experimental results will be reported elsewhere [70], together with evidence that our SLM-pumped, TDL-seeded PPLN OPO [19, 20] also yields high-quality CRD spectra.

It should be noted that the vertical response of the CRD spectrum presented in Fig. 5 is not perfectly linear when a comparison is made with the HITRAN simulation: the strongest peaks in the spectrum are reduced in amplitude by as much as 60% relative to the weakest peaks. Stronger peaks in the spectrum with shorter ringdown times appear to be less well determined than the weaker, such that the lower-amplitude portions of the spectrum (6450–6475 cm^{-1} and 6530–6560 cm^{-1}) display excellent vertical linearity. This effect may be due in part to the limited 8-bit vertical resolution and 1000-point sampling capacity of the digital oscilloscope used. The relatively large scan-step interval ($\sim 0.04\,cm^{-1}$) of the wide-ranging survey spectrum in Fig. 5 may also be a limitation. However, we believe that the dominant cause of the nonlinear CRD response is attributable to the weak broadband pedestal underlying the intense narrowband component of our TDL-seeded OPO radiation, as characterised above. Broadband pedestal effects are not unusual in injection-seeded OPOs, becoming more pronounced as the power of seed radiation is decreased. It is not clear at this stage whether the pedestal is aggravated by the use of a MM pump laser, rather than a SLM pump laser as in our previous PPLN OPO experiments [19, 20]. Such pedestal effects need to be treated with particular care in CRD applications, for they can cause the ringdown curves to become multi-exponential and thus complicate the applicability of the simple CRD curve-fitting algorithm that we prefer to use. The importance of correctly accounting for complicated laser spectral profiles (and associated failure of the single-exponential-decay approximation) has previously been recognised in the general context of CRD spectroscopy [76, 80]. The following discussion provides a pronounced instance of this problem, as a cautionary tale.

We have also taken a more conventional approach to IR CRD spectroscopy, using our Mirage 3000 OPO/OPA system, in the course of experiments on van der Waals molecules incorporating C_2H_2. The CRD apparatus employs a much larger, higher-performance tunable IR source, but is otherwise similar to that described above with several variations:

- the sample chamber is a molecular beam apparatus evacuated by a diffusion pump (Varian VHS-6) and Roots blower (Alcatel 113), with a pulsed slit nozzle (General Valve 009-0534-900; aperture 0.125 × 125 mm) creating a supersonic free jet of C_2H_2 molecules;

- the ringdown cavity (~ 0.3 m long) is mounted inside the vacuum chamber, with motorised micropositioners (New Focus 8809-V) controlling mirror alignment;
- an InSb detector (Cincinnati Electronics SSD1963), cooled by liquid nitrogen, replaces the InGaAs photodiode used in the CRD experiments described above;
- a photoacoustic reference channel is provided, with a cylindrical PA gas cell containing the molecule of interest as a calibrant.

Spectroscopic results obtained with this apparatus are presented in Fig. 6. It shows a pair of 10-cm^{-1} scans of spectra near the 6556.4-cm^{-1} origin of the $(\nu_1 + \nu_3)$ rovibrational combination band of C_2H_2 [81]. The upper trace is the IR CRD spectrum obtained in a slit jet of C_2H_2 gas expanded from a stagnation pressure of 1 bar with a solenoid-valve opening time of 450 μs; the observed FWHM linewidth is ~ 0.02 cm^{-1} (600 MHz). The lower (inverted) trace is a simultaneously recorded PA spectrum for ~ 40 Torr of C_2H_2 gas. These spectra reveal rovibrational features that are attributable to the $(\nu_1 + \nu_3)$ bands of $^{12}C_2H_2$ and $^{12}C^{13}CH_2$ (designated by grids at the top of Fig. 6) as well as $(\nu_1 + \nu_3 + \nu_4 - \nu_4)$ hot bands. Some of the intensity differences are readily understood in terms of the low rotational temperature of C_2H_2 molecules in the supersonic free jet. However, features due to $^{12}C^{13}CH_2$ are much stronger in the CRD spectrum than is expected on the basis of the 1.1% natural abundance of ^{13}C. It is implausible that some exotic form of isotope enrichment could occur in the expanding gas or that the $^{12}C_2H_2$ transitions are undergoing selective optical saturation. The explanation of the intensity anomalies is in fact more mundane, as we now explain.

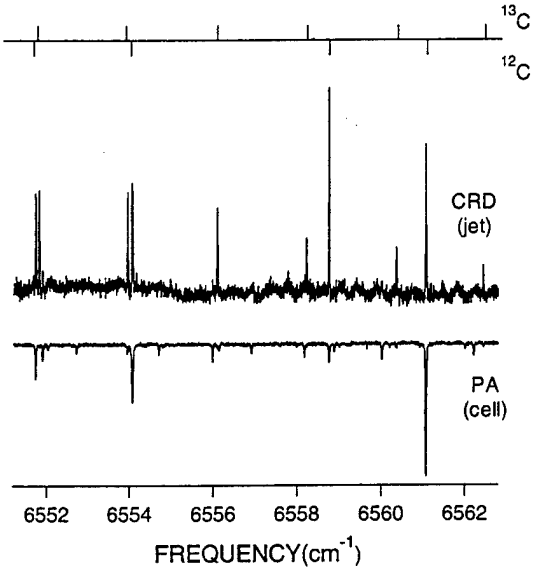

Fig. 6. Rovibrational IR absorption spectra at ~ 6555 cm^{-1} (1.525 μm) for C_2H_2 molecules, each recorded by continuously scanning the narrowband output wavelength of a Mirage 3000 OPO/OPA system. The upper trace is a CRD spectrum for a supersonic free jet of C_2H_2 expanded through a pulsed slit nozzle from a stagnation pressure of 1 bar. The lower trace is a corresponding PA spectrum for C_2H_2 gas ($T = 300$ K, $P = 40$ Torr). Features due to $^{12}C^{13}CH_2$ (1.1% natural abundance) are much more intense than expected relative to those for $^{12}C_2H_2$, for reasons that are discussed in the text and explored further in Fig. 7

We infer that, under the operating conditions employed here, the Mirage 3000 IR output also has a weak broadband component in addition to the strong narrowband tunable output. This again causes the ringdown curves to be multiexponential, so that our CRD curve-fitting algorithm needs to be used with caution. This is demonstrated in Fig. 7, which shows pairs of on- and off-resonance ringdown curves (upper and lower curves, respectively) that are sampled in two different time zones: (a) late and (b) early, as designated by bold curves. Trace (c) shows that 'late' sampling as in (a) yields severe intensity discrepancies in the relative amplitudes of the two features designated A and B, which correspond to 6551.7-cm^{-1} $^{12}C_2H_2$ P(2) and 6551.8-cm^{-1} $^{12}C^{13}CH_2$ R(3), respectively; this situation is similar to that in Fig. 6. Trace (d) corresponds to the 'early' mode of sampling (b), where the same two $^{12}C_2H_2$ P(2) and $^{12}C^{13}CH_2$ R(3) rovibrational features (designated A′ and B′) now have more realistic relative amplitudes. It is evident that the on-resonance ringdown curves, as in the lower curves of Fig. 7a and b, comprise a narrowband, rapidly decaying (attenuated) component superimposed on a broadband, slowly decaying (unattenuated) component. The separation of these two components (wanted and unwanted, respectively) is then a matter of trade-off between simplicity/efficiency of the CRD curve-fitting algorithm and the scan rate and signal-to-noise ratio with which high-resolution CRD spectra can be faithfully recorded.

2.3 Time-resolved IR-UV DR spectroscopy

One of the original objectives of our programme of tunable OPO development was to devise convenient tunable, narrowband coherent sources of ns-pulsed IR and UV radiation for time-resolved, LIF-detected infrared–ultraviolet double resonance (IR-UV DR) experiments on the spectroscopy and energy-transfer dynamics of small gas-phase polyatomic molecules such as C_2H_2 [82–84]. An injection-seeded BBO OPO was previously used to record UV-scanned IR-UV DR spectra of the '$3\nu_{CH}$' manifold of C_2H_2 at ~ 9600 cm^{-1} [4, 11].

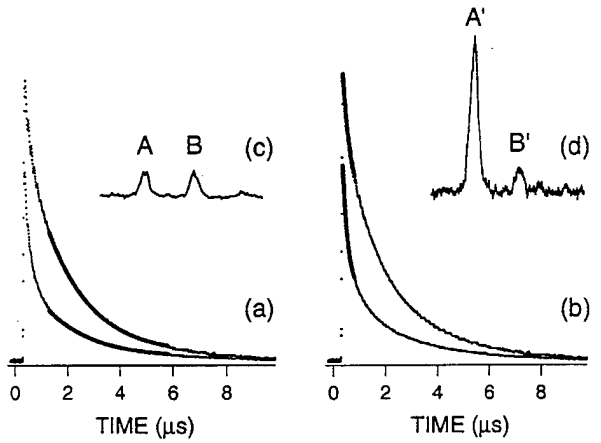

Fig. 7. Two different forms of curve-fitting (a, b) for on- and off-resonance CRD decay curves for the 6551.7-cm^{-1} P(2) rovibrational feature of $^{12}C_2H_2$, with the time zones sampled by the curve-fitting algorithm marked by *bold lines*. Corresponding CRD spectra (c, d) show features (A, A′) and (B, B′) at 6551.7-cm^{-1} and 6551.8-cm^{-1}, due to $^{12}C_2H_2$ P(2) and $^{12}C^{13}CH_2$ R(3) respectively for the two different sampling regimes; the latter (b, d) is more realistic

We now report IR-scanned IR-UV DR spectra of the '$4\nu_{CH}$' manifold of C_2H_2 at $\sim 12\,700\,cm^{-1}$, by using the Mirage 3000 OPO/OPA system (see Sect. 1.4) as a continuously tunable narrowband IR PUMP source and, as UV PROBE source, the OPO/SFG system (see Sect. 1.6, Fig. 2, and the second column of Table 1) tuned to a fixed, characteristic rovibronic transition. The TDL seed laser (New Focus 6262) spans the range 1.50–1.59 μm (~ 1.51 μm used here). The Mirage 3000 system has an effective scanning bandwidth of $< 0.017\,cm^{-1}$, five times narrower than the $0.08\text{-}cm^{-1}$ bandwidth of the Raman-shifted, Nd:YAG-pumped dye laser system regularly used as IR PUMP source in our IR-UV DR experiments [82–84]. Likewise, the $\sim 0.06\text{-}cm^{-1}$ optical bandwidth of the OPO/SFG UV output offers a five-fold advantage relative to the $\sim 0.3\text{-}cm^{-1}$ bandwidth of the excimer-pumped, frequency-doubled dye laser system that is our regular UV PROBE LIF-excitation source [82–84]. Corresponding Doppler widths for the IR and UV transitions of interest here are $0.03\,cm^{-1}$ and $0.075\,cm^{-1}$, respectively, each exceeding the optical bandwidth of the corresponding narrowband OPO source considered. A tableau of representative results is presented in Fig. 8, comparing IR-UV DR spectra obtained with the various IR PUMP and UV PROBE options.

Traces (a)–(c) of Fig. 8 are IR-UV DR spectra of the $(\nu_1 + 3\nu_3)$ rovibrational band of C_2H_2 gas ($T = 300$ K, $P = 0.2$ Torr), with the regular IR PROBE source scanned and the UV PROBE source (either regular or OPO/SFG) tuned to a single rovibronic transition at 323.00 nm that is known [84] to be characteristic of the $V_1 = 1$, $V_3 = 3$, $J = 19$ rovibrational level of C_2H_2. Trace (a) is recorded with short IR-UV delay interval (10 ns) to produce effectively collision-free conditions with Lennard–Jones collision number $z = 0.033$. Traces (b) and (c) are recorded with a 20-fold increase in IR-UV delay (200 ns) and collision number ($z = 0.66$), which causes collision-induced rovibrational satellite structure to appear. Some of this is attributable to commonplace even-$|\Delta J|$ rotational energy transfer, but other features – most notably that designated R(11)† – correspond to normally forbidden odd-$|\Delta J|$ energy transfer [82, 83] that remains a topic of considerable current curiosity and ongoing research [84, 85]. Trace (c) differs from (b) in that the regular UV PROBE source is replaced by the narrower-band OPO/SFG source. Likewise, the regular tunable IR PUMP source used to record trace (c) is replaced in the case of trace (d) by the narrower-band Mirage 3000 OPO/OPA system. Traces (e) and (f) show corresponding IR PA spectra, inverted for reference purposes and with $P(C_2H_2) = 30$ Torr. Not unexpectedly, the resolution of traces (d) and (f) is clearly superior to that in traces (a)–(c) and (e). The close similarity between traces (b), (c), and (d) reassures us that, at least in this case, the relatively broad optical bandwidths of the regular IR PROBE and UV PROBE sources have not obscured any fine state-resolution issues that might have had significant mechanistic implications.

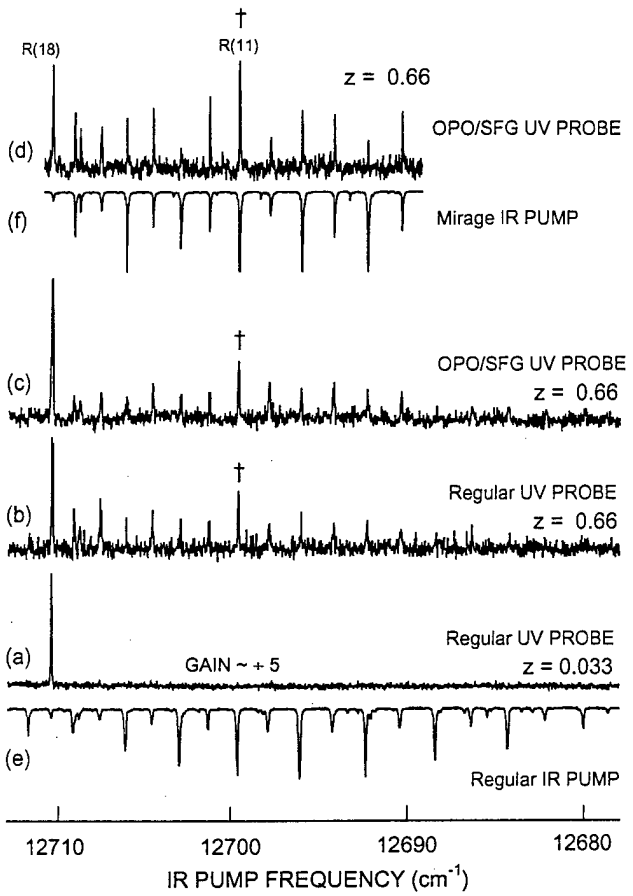

Fig. 8. Time-resolved, LIF-detected IR-UV DR spectra (a–d) and corresponding IR PA reference spectra (e, f) recorded by scanning a tunable IR source through the R branch of the $(\nu_1 + 3\nu_3)$ rovibrational band of C_2H_2 gas. Each IR-UV DR spectrum is obtained with the UV PROBE source tuned to a rovibronic transition at 323.00 nm that is characteristic of the $V_1 = 1$, $V_3 = 3$, $J = 19$ rovibrational level of C_2H_2. Trace (a) corresponds to collision-free conditions with Lennard–Jones collision number $z = 0.033$, whereas traces (b–d) have $z = 0.66$ and display collision-induced rovibrational energy transfer satellite structure, both regular even-$|\Delta J|$ and normally forbidden odd-$|\Delta J|$. In traces (c) and (d), the regular UV PROBE source is replaced by the OPO/SFG tunable UV source depicted in Fig. 2. In traces (d) and (f), the regular IR PUMP source is replaced by a Mirage 3000 OPO/OPA tunable IR source

2.4 OPO-based UV LIF sensing of nitric oxide

Nitric oxide (NO) is a significant chemical species in many high-temperature, atmospheric, combustion, and flow-dynamic processes [86]. It is also a prominent product molecule in laser-induced photochemistry [87]. We aim to extend our tunable OPO methodology as a viable solid-state alternative to excimer lasers in spatially resolved UV-spectroscopic imaging of NO concentration and temperature distributions in combustion media such as flames, furnaces, and automobile engines, or in characterising energy disposal in photofragmentation reactions. The OPO option is particularly realistic for combustion-diagnostic methods that require only moderate UV intensity and are restricted by the limited tunability of excimer lasers or by the efficiency of excimer-pumped dye lasers. For instance, we envisage that the tunable OPO/SFG system described in Sect. 1.6 above could facilitate imaging of NO concentrations in combustion media, by two-dimensional LIF detection in a planar-sheet focus. The UV wavelengths required are 225–227 nm for the strong 0-0 band in the A-X absorption system of NO and 246–248 nm for the weaker 0-2 hot band. Elaborate Raman-shifted and dye-laser-seeded tunable KrF excimer laser systems have

been used to generate these respective wavelengths in previous UV LIF studies of NO [88].

The OPO/SFG system described in Sect. 1.6 and Fig. 2 above represents a preliminary step in this direction. The design parameters outlined in the third and fourth columns of Table 1 enable the two key wavelength regions of the 0-0 and 0-2 bands of NO to be accessed with a single external-cavity diode laser (New Focus 6227) tunable over the range 814–837 nm, a single BBO OPO crystal (cut at 30° for Type-I phase matching), and a single BBO SFG crystal (cut at 53° for Type-I phase matching). The only adjustments that need to be made to switch the UV output of this system between the regions of the NO 0-0 and 0-2 bands entail tuning the TDL seed wavelength between ~ 824 nm and ~ 814 nm, altering the phase-matching angles of the BBO OPO and SFG crystals to pre-determined settings, and interchanging several dichroic optical elements.

The spectroscopic potential of the OPO/SFG system in this context is demonstrated in Fig. 9a, which presents a UV LIF excitation spectrum of the 226-nm Q branch in the 0-0 band of NO gas ($T = 300$ K, $P = 0.25$ Torr), recorded with the BBO OPO pumped at ~ 100 mJ/pulse (~ 2.5 times its operating threshold). The UV SFG energy incident on the sample is attenuated to ~ 0.1 mJ/pulse to avoid optical saturation. In recording this spectrum, the OPO ring-cavity length was asynchronously dithered by means of a piezoelectric mirror mount; this is a customary way [16, 18] to randomise and average out intensity and spatial variations that arise as the passive, TDL-seeded OPO is tuned. The simulated spectrum in Fig. 9b (generated by the LIFBASE spectral code [89]) is in satisfactory agreement with Fig. 9a, apart from amplitude discrepancies that are attributable to shot-to-shot variations of OPO and SFG output intensities and to the fact that neither of the BBO phase-matching angles is optimally adjusted in the course of this 2-cm^{-1} spectroscopic scan. The observed linewidth in Fig. 9a is $\sim 0.115\,cm^{-1}$ FWHM, corresponding to a convolution of the 0.100-cm^{-1} Doppler width of NO with the $0.06\,cm^{-1}$ effective scanning bandwidth of the OPO/SFG UV output [84]. This UV bandwidth is sub-Doppler for bulk NO gas at temperatures above ~ 110 K, and in this sense is therefore narrower-band than it needs to be. However, such narrowband radiation is useful for applications where the Doppler profile cannot be predicted, such as determining translational energy disposal in NO fragments produced by exothermic photodissociation reactions involving photolysis by pulsed excimer lasers [87].

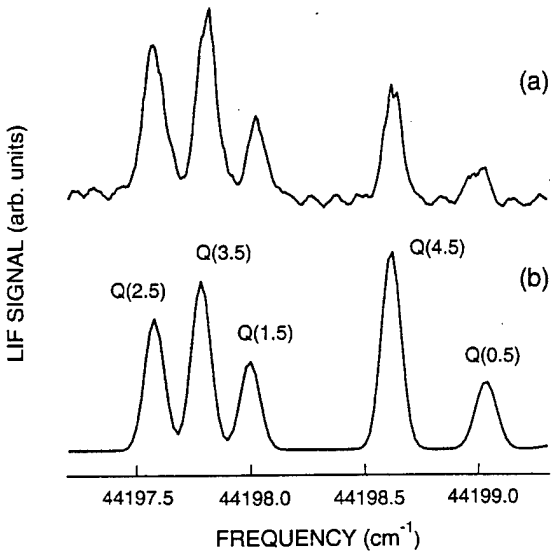

Fig. 9. Rovbronic spectra of the 226-nm Q branch in the 0-0 band of the *A-X* electronic absorption system of NO. Trace (a) is a UV LIF excitation spectrum of NO gas ($T = 300$ K, $P = 0.25$ Torr), recorded with the TDL-seeded BBO OPO/SFG spectroscopic system depicted in Fig. 2. Operating parameters are as in the third column of Table 1, except that the UV SFG pulse energy incident on the sample is attenuated to ~ 0.1 mJ to avoid optical saturation. Trace (b) is a corresponding simulated spectrum, generated by the LIFBASE spectral code [89] with rovibronic features designated as Q(*J*)

It is evident that UV LIF detection of NO is just one of many spectroscopic sensing applications for which our tunable OPO/SFG system is well suited. We note in particular its potential to compete successfully with frequency-doubled or SFG dye lasers for sensitive, high-resolution spectroscopic detection of NO by DFWM [65, 90].

3 Concluding remarks: future prospects

The message of this paper concerns the variety of instrumental strategies, some less conventional than others, involved in ns-pulsed, continuously tunable OPO/OPA systems that are useful for spectroscopic sensing of chemical processes in laboratory, industrial, and environmental settings. Our research in this area [4, 9–20, 70–73] is closely linked to actual spectroscopic studies, not only for the purpose of spectroscopic sensing *per se* but also to provide realistic performance tests for tunable OPO/OPA systems under development.

Issues that need to be highlighted include the utility of modular, injection-seeded tunable OPO/OPA systems, in which the wavelength-control function is separated from the optical power-generation function. The injection-seeding approach has some advantages in terms of performance and convenience, relative to more conventional OPO-tuning strategies based simply on phase-matching conditions or on intra-cavity gratings and étalons. This paper has surveyed the relative merits of several such designs of ns-pulsed, tunable OPO/OPA system, spanning a wide range of operational complexity.

At one extreme is our TDL-seeded PPLN OPO/OPA system [19, 20] that uses active 'intensity-dip' cavity control and provides an effective scanning optical bandwidth of 130 ± 10 MHz ($0.0043 \pm 0.0003\,cm^{-1}$). This compares favourably with the optical bandwidth of advanced grating-tuned OPO/OPA systems [32, 67, 68], although the continuous scanning range of the injection-seeded system is more restricted owing to TDL and QPM limitations.

A key feature of this paper (in Sects. 1.4 and 2.2) is the use of a simple, inexpensive, compact MM Nd:YAG laser as the pump source for a TDL-seeded PPLN OPO with the same form of active cavity control as above [19, 20]. It is remarkable that it is still possible to obtain continuously tunable single-mode signal output from this much simpler MM-pumped system, with an effective scanning bandwidth ($\sim 0.005\,cm^{-1}$) that is comparable to that of the SLM-pumped PPLN OPO [19, 20]. This offers the prospect of a compact, transportable OPO system suitable for spectroscopic sensing in the field or at industrial sites. Admittedly,

the amplitude stability of radiation from this TDL-seeded, MM-pumped PPLN OPO is inferior (by up to an order of magnitude [70]) to that pumped by a more elaborate single-mode Nd:YAG laser [19, 20] but that does not impede acceptable spectroscopic performance.

For instance, the TDL-seeded, MM-pumped OPO lends itself to high-resolution CRD spectroscopy, as illustrated in Fig. 5. The noise-limited absorbance sensitivity attained ($< 10^{-7}\,cm^{-1}$) is highly satisfactory. However, such spectra provide evidence that the narrowband component of OPO signal output is accompanied by a weak, broadband pedestal. Although this pedestal has very low spectral irradiance (< 1% of the narrowband component), its wavelength-integrated pulse energy is appreciable ($\leq$ 50% of total energy) and tends to complicate the real-time analysis of CRD signals by introducing multi-exponential ringdown decay. An exaggerated case of this type of complication is addressed in Figs. 6 and 7, corresponding to CRD spectroscopy with a large commercial grating-tuned OPO/OPA system.

In a less elaborate approach, convenient continuous narrowband tunability can be achieved passively by using a slightly misaligned OPO cavity with a low effective finesse that enables slightly non-collinear phase-matching and operation on a variety of transverse modes of the OPO cavity [9–12, 14–18]. Further examples of this strategy have been presented in Sects. 1.5, 2.1, and 2.4. This method is employed in the TDL-seeded OPO/SFG UV-spectroscopic systems described in Sect. 1.6 and employed to record time-resolved IR-UV DR spectra of C_2H_2 gas (Sect. 2.3) and UV LIF spectra of NO gas (Sect. 2.4).

The passive, misaligned-cavity method of injection-seeded OPO wavelength control is also useful for multi-wavelength spectroscopic tailoring. This approach has so far been applied [16, 17] to a passive-cavity BBO OPO, simultaneously injection-seeded by two distinct TDLs. Such a system has been employed for OPO-based multiplex CARS thermometry of nitrogen in furnace air [16]. Other results in this context await publication [72, 73].

We consider that spectroscopic tailoring methods have great potential for multiplex spectroscopic sensing. This approach uses a coherent, pulsed light source (for example, an OPO) to generate a set of discrete wavelengths that are controlled to match characteristic features in spectra of molecular target species in a given sensing application, either laboratory-based or remote (for example, IR DIAL monitoring of atmospheric species [22]). Each narrowband component of this tailored set of wavelengths ultimately needs to be computer-addressable and capable of modulation in ways that enable decoding of resulting spectroscopic signals, with a multiplex advantage for detection sensitivity and specificity.

Prospective developments such as these indicate that ns-pulsed tunable OPOs can play a significant role in future spectroscopic sensing technology, including applications in the fields of combustion diagnostics and chemical dynamics where Jürgen Wolfrum and his colleagues have made an indelible mark [91].

Acknowledgements. Daniel Roberts and Philip Burns assisted with some of the spectroscopic measurements of NH_3 and CO_2, respectively. We acknowledge financial support from the Australian Research Council and Macquarie University. J. Nibler thanks Macquarie University, Oregon State University, and the National Science Foundation for research support during a sabbatical period in 1998.

References

1. R.L. Byer: In *Quantum Electronics: A Treatise, Volume I, Nonlinear Optics*, Part B, ed. by H. Rabin, C.L. Tang (Academic Press, New York 1975) pp. 587–702
2. R.L. Byer, R.L. Herbst: In *Nonlinear Infrared Generation*, ed. by Y.-R. Shen (Springer, New York 1977) pp. 81–137
3. S.J. Brosnan, R.L. Byer: IEEE J. Quantum Electron. **QE-15**, 415 (1979)
4. B.J. Orr, M.J. Johnson, J.G. Haub: In *Tunable Laser Applications*, ed. by F.J. Duarte (Marcel Dekker, New York 1995) pp. 11–82
5. A. Fix, T. Schröder, R. Wallenstein: Laser Optoelektronik **23**(3), 106 (1991)
6. C.L. Tang, W.R. Bosenberg, T. Ukachi, R.J. Lane, L.K. Cheng: Proc. IEEE **80**, 365 (1992)
7. N.P. Barnes: In *Tunable Lasers Handbook*, ed. by F.J. Duarte (Academic Press, San Diego 1995) pp. 293–348
8. M. Ebrahimzadeh, R.C. Eckardt, M.H. Dunn: J. Opt. Soc. Am. B **16**, 1477 (1999); this introduces a special issue on "Optical Parametric Devices and Processes"
9. J.G. Haub, M.J. Johnson, B.J. Orr, R. Wallenstein: Appl. Phys. Lett. **58**, 1718 (1991)
10. A. Fix, T. Schröder, R. Wallenstein, J.G. Haub, M.J. Johnson, B.J. Orr: J. Opt. Soc. Am. B **10**, 1744 (1993)
11. J.G. Haub, M.J. Johnson, B.J. Orr: J. Opt. Soc. Am. B **10**, 1765 (1993)
12. M.J. Johnson, J.G. Haub, H.-D. Barth, B.J. Orr: Opt. Lett. **18**, 441 (1993)
13. J.G. Haub, M.J. Johnson, A.J. Powell, B.J. Orr: Opt. Lett. **20**, 1637 (1995)
14. M.J. Johnson, J.G. Haub, B.J. Orr: Opt. Lett. **20**, 1277 (1995)
15. J.G. Haub, R.M. Hentschel, M.J. Johnson, B.J. Orr: J. Opt. Soc. Am. B **12**, 2128 (1995)
16. G.W. Baxter, M.J. Johnson, J.G. Haub, B.J. Orr: Chem. Phys. Lett. **251**, 211 (1996)
17. G.W. Baxter, J.G. Haub, B.J. Orr: J. Opt. Soc. Am. B **14**, 2723 (1997)
18. G.W. Baxter, H.-D. Barth, B.J. Orr: Appl. Phys. B **66**, 653 (1998)
19. G.W. Baxter, Y. He, B.J. Orr: Appl. Phys. B **67**, 753 (1998)
20. Y. He, G.W. Baxter, B.J. Orr: Rev. Sci. Instrum. **70**, 3203 (1999)
21. S. Svanberg: In *Air Monitoring by Spectroscopic Techniques*, ed. by M.W. Sigrist (Wiley, New York 1994) pp. 85–161; W.B. Grant: In *Tunable Laser Applications*, ed. by F.J. Duarte (Marcel Dekker, New York 1995) pp. 231–245
22. B.J. Orr: "IR lidar applications in air monitoring", accepted for publication in Encyclopedia of Analytical Chemistry: Instrumentation and Applications, ed. by R.A. Myers (Wiley, Chichester, UK 2000)
23. T. Henningsen, M. Garbuny, R.L. Byer: Appl. Phys. Lett. **24**, 242 (1974); R.A. Baumgartner, R.L. Byer: Opt. Lett. **2**, 163 (1978); R.A. Baumgartner, R.L. Byer: Appl. Opt. **17**, 3555 (1978); M. Endemann, R.L. Byer: Opt. Lett. **5**, 452 (1980); D.J. Brassington: Appl. Opt. **21**, 4411 (1982)
24. V.G. Dmitriev, G.G. Gurzayan, D.N. Nikogosyan: *Handbook of Nonlinear Optical Crystals*, 2nd edn. (Springer, Berlin, Heidelberg 1997)
25. W. Koechner: *Solid-State Laser Engineering*, 4th edn. (Springer, Berlin, Heidelberg 1996)
26. M.J.T. Milton, T.D. Gardiner, F. Molero, J. Galech: Opt. Commun. **142**, 153 (1997)
27. G. Ehret, A. Fix, V. Weiss, G. Poberaj, T. Baumert: Appl. Phys. B **67**, 427 (1998)
28. A. Fix, V. Weiss, G. Ehret: Pure Appl. Opt. **7**, 837 (1998)
29. W.R. Bosenberg, A. Drobshoff, J.I. Alexander, L.E. Myers, R.L. Byer: Opt. Lett. **20**, 52 (1995); L.E. Myers, R.C. Eckardt, M.M. Fejer, R.L. Byer, W.R. Bosenberg, J.W. Pierce: J. Opt. Soc. Am. B **12**, 2102 (1995)
30. L.E. Myers, R.C. Eckardt, M.M. Fejer, R.L. Byer, W.R. Bosenberg: Opt. Lett. **21**, 591 (1996)
31. D.W. Michael, K. Kolenbrander, J.M. Lisy: Rev. Sci. Instrum. **57**, 1210 (1986); T.K. Minton, S.A. Reid, H.L. Kim, J.D. McDonald: Opt. Commun. **69**, 289 (1989)
32. W.R. Bosenberg, D.R. Guyer: J. Opt. Soc. Am. B **10**, 1716 (1993)
33. L.A.W. Gloster, I.T. McKinnie, Z.X. Jiang, T.A. King, J.M. Boon-Engering, W.E. van der Veer, W. Hogervorst: J. Opt. Soc. Am. B **12**, 2117 (1995); J.M. Boon-Engering, L.A.W. Gloster, W.E. van der Veer, I.T. McKinnie, T.A. King, W. Hogervorst: Opt. Lett. **20**, 2087 (1995)

34. F. Huisken, M. Kaloudis, J. Marquez, Y L. Chuzavkov, S.N. Orlov, Y.N. Polivanov, V.V. Smirnov: Opt. Lett. **20**, 2306 (1995)
35. P. Schlup, S.D. Butterworth, I.T. McKinnie: Opt. Commun. **154**, 191 (1998); P. Schlup, I.T. McKinnie, S.D. Butterworth: Appl. Opt. **38**, 7398 (1999)
36. S.T. Yang, S.P. Velsko: Opt. Lett. **24**, 133 (1999)
37. C.-S. Yu, A.H. Kung: J. Opt. Soc. Am. B **16**, 2233 (1999)
38. D.F. Plusquellic, O. Votava, D.J. Nesbitt: Appl. Opt. **35**, 1464 (1996); O. Votava, J.R. Fair, D.F. Plusquellic, E. Riedle, D.J. Nesbitt: J. Chem. Phys. **107**, 8854 (1997)
39. M.J.T. Milton, T.D. Gardiner, G. Chourdakis, P.T. Woods: Opt. Lett. **19**, 281 (1994)
40. J.M. Boon-Engering, W.E. van der Veer, J.W. Gerritsen, W. Hogervorst: Opt. Lett. **20**, 380 (1995)
41. N. Srinivasan, T. Kimura, H. Kiriyama, M. Yamanaka, Y. Izawa, S. Nakai, C. Yamanaka: Jpn. J. Appl. Phys. **35**, 3457 (1996)
42. P. Bourdon, M. Péalat, V.I. Fabelinsky: Opt. Lett. **20**, 474 (1995); P. Bourdon, M. Péalat: Quantum Semiclass. Opt. **9**, 269 (1997)
43. A. Fix, R. Wallenstein: J. Opt. Soc. Am. B **13**, 2484 (1996); A. Borsutzky: Quantum Semiclass. Opt. **9**, 191 (1997)
44. P. Schlup, N.A. Russell, I.T. McKinnie, S.D. Butterworth, A. Oien, D.M. Warrington: Proc. SPIE **3265**, 265 (1998)
45. D.C. Hovde, J.H. Timmermans, G. Scoles, K.K. Lehmann: Opt. Commun. **86**, 294 (1991)
46. F. Huisken, A. Kulcke, D. Voelkel, C. Laush, J.M. Lisy: Appl. Phys. Lett. **62**, 805 (1993)
47. T.D. Raymond, W.J. Alford, A.V. Smith, M.S. Bowers: Opt. Lett. **19**, 1520 (1994); A.V. Smith, W.J. Alford, T.D. Raymond, M.S. Bowers: J. Opt. Soc. Am. B **12**, 2253 (1995)
48. W.A. Neuman, S.P. Velsko: Proceedings of International Conference on Lasers '95, ed. by V.J. Corcoran, T.A. Goldman (STS Press, Society for Optical and Quantum Electronics, McLean, Virginia, 1996) pp. 718–725; M.S. Webb, K.B. Stanion, D.J. Deane, W.A. Cook, W.A. Neuman, S.P. Velsko: Proc. SPIE **2700**, 269 (1996)
49. A. Borsutzky, R. Bruenger, R. Wallenstein: Appl. Phys. B **52**, 380 (1991)
50. B.C. Johnson, V.J. Newell, J.B. Clark, E.S. McPhee: J. Opt. Soc. Am. B **12**, 2122 (1995)
51. A. Fix, G. Ehret: Appl. Phys. B **67**, 331 (1998)
52. R.A. Baumgartner, R.L. Byer: IEEE J. Quantum Electron. **QE-15**, 432 (1979)
53. A. Agnesi, E. Piccinini, G.C. Reali, C. Solcia: Appl. Phys. B **65**, 303 (1997)
54. H. Karlsson, M. Olson, G. Arvidsson, F. Laurell, U. Bäder, A. Borsutzky, R. Wallenstein, S. Wickström, M. Gustafsson: Opt. Lett. **24**, 330 (1999)
55. R.S. Conroy, C.F. Rae, M.H. Dunn, B.D. Sinclair, J.M. Ley: Opt. Lett. **24**, 1614 (1999)
56. G.W. Baxter, P. Schlup, I.T. McKinnie: Appl. Phys. B **70**, 301(2000)
57. S.A. Reid, Y. Tang: Appl. Opt. **248**, 476 (1996); Y. Tang, S.A. Reid: Chem. Phys. Lett. **248**, 476 (1996)
58. P.E. Powers, T.W. Aniolek, T.J. Kulp, B.A. Richman, S.E. Bisson: Opt. Lett. **23**, 1886 (1998); K.W. Aniolek, P.E. Powers, T.J. Kulp, B.A. Richman, S.E. Bisson: Chem. Phys. Lett. **302**, 555 (1999)
59. U. Bäder, J.-P. Meyn, J. Bartschke, T. Weber, A. Borsutzky, R. Wallenstein, R.G. Batchko, M.M. Fejer, R.L. Byer: Opt. Lett. **24**, 1608 (1999)
60. M. Ebrahimzadeh, A.J. Henderson, M.H. Dunn: IEEE J. Quantum Electron. **QE-26**, 1241 (1990)
61. L.A.W. Gloster, I.T. McKinnie, T.A. King: Opt. Commun. **112**, 328 (1994); L.A.W. Gloster, Z.X. Jiang, T.A. King: IEEE J. Quantum Electron. **QE-30**, 2961 (1994); A.L. Oien, I.T. McKinnie, P. Jain, N.A. Russell, D.M. Warrington, L.A.W. Gloster: Opt. Lett. **22**, 859 (1997)
62. Y. Tang, C.F. Rae, C. Rahlff, M.H. Dunn: J. Opt. Soc. Am. B **14**, 3442 (1997)
63. R. Urschel, U. Bäder, A. Borsutzky, R. Wallenstein: J. Opt. Soc. Am. B **16**, 565 (1999)
64. A.V. Smith, R.J. Gehr, M.S. Bowers: J. Opt. Soc. Am. B **16**, 609 (1999); W.J. Alford, R.J. Gehr, R.L. Schmitt, A.V. Smith, G. Arisholm: J. Opt. Soc. Am. B **16**, 1525 (1999)
65. G. Hansson, D.D. Smith: Appl. Opt. **37**, 5743 (1998); P.E. Britton, D. Taverner, K. Puech, D.J. Richardson, P.G.R. Smith, G.W. Ross, D.C. Hanna: Opt. Lett. **23**, 582 (1998); P.E. Britton, H.L. Offerhaus, D.J. Richardson, P.G.R. Smith, G.W. Ross, D.C. Hanna: Opt. Lett. **24**, 975 (1999)
66. R.L. Farrow, D.J. Rakestraw: Science **257**, 1894 (1992)
67. R.L. Vander Wal, B.E. Holmes, J.B. Jeffries, P.M. Danehy, R.L. Farrow, D.J. Rakestraw: Chem. Phys. Lett. **191**, 251 (1992); G.J. Germann, T. Dreier, R.L. Farrow, D.J. Rakestraw: Ber. Bunsenges. Phys. Chem. **97**, 1630 (1993); G.J. Germann, R.L. Farrow, D.J. Rakestraw: J. Opt. Soc. Am. B **12**, 25 (1995)
68. J.J. Scherer, D. Voelkel, D.J. Rakestraw, J.B. Paul, C.P. Collier, R.J. Saykally, A. O'Keefe: Chem. Phys. Lett. **245**, 273 (1995); J.J. Scherer, D. Voelkel, D.J. Rakestraw: Appl. Phys. B **64**, 699 (1997)
69. D. Voelkel, Y.L. Chuzavkov, J. Marquez, S.N. Orlov, Y.N. Polivanov, V.V. Smirnov, F. Huisken: Appl. Phys. B **65**, 93 (1997)
70. Y. He, B.J. Orr: to be published
71. M.J. Johnson: PhD Thesis (Macquarie University, Sydney, Australia 1995)
72. G.W. Baxter: PhD Thesis (Macquarie University, Sydney, Australia 1998)
73. G.W. Baxter, J.G. Haub, Y. He, M.J. Johnson, B.J. Orr: to be published
74. R. Urschel, A. Borsutzky, R. Wallenstein: Appl. Phys. B. **70**, 203 (2000)
75. L. Lundsberg-Nielsen, F. Hegelund, F.M. Nicolaisen: J. Molec. Spectrosc. **162**, 230 (1993)
76. J.J. Scherer, J.B. Paul, A. O'Keefe, R.J. Saykally: Chem. Rev. **97**, 25 (1997); J.B. Paul, R.J. Saykally: Analyt. Chem. **69**, 287A (1997); M.D. Wheeler, S.M. Newman, A.J. Orr-Ewing, M.N.R. Ashfold: J. Chem. Soc. Faraday Trans. **94**, 337 (1998); K.W. Busch, M.A. Busch (Ed.): Cavity-Ringdown Spectroscopy – An Ultratrace-Absorption Measurement Technique, ACS Symposium Series No. 720 (Oxford University Press 1999)
77. Y. He, B.J. Orr: Chem. Phys. Lett. **319**, 131 (2000)
78. L.S. Rothman, C.P. Rinsland, A. Goldman, S.T. Massie, D.P. Edwards, J.-M. Flaud, A. Perrin, C. Camy-Peyret, V. Dana, J.-Y. Mandin, J. Schroeder, A. McCann, R.R. Gamache, R.B. Watson, K. Yoshino, K.V. Chance, K.W. Jucks, L.R. Brown, V. Nemtchinov, P. Varanasi: J. Quant. Spectrosc. Radiat. Transfer **60**, 665 (1998)
79. C.-P. Courtoy: Canad. J. Phys. **35**, 608 (1957); R.A. Toth, R.H. Hunt, E.K. Plyler: J. Molec. Spectrosc. **38**, 107 (1971)
80. J.T. Hodges, J.P. Looney, R.D. van Zee: Appl. Opt. **35**, 4112 (1996)
81. Q. Kou, G. Guelachvili, M. Abboutti Temsamami, M. Herman: Canad. J. Phys. **72**, 1241 (1994)
82. A.P. Milce, H.-D. Barth, B.J. Orr: J. Chem. Phys. **100**, 2398 (1994); A.P. Milce, B.J. Orr: J. Chem. Phys. **104**, 6423 (1996); **106**, 3592 (1997)
83. M.A. Payne, A.P. Milce, M.J. Frost, B.J. Orr: Chem. Phys. Lett. **265**, 244 (1997)
84. M.A. Payne: PhD Thesis (Macquarie University, Sydney, Australia 1999)
85. A.P. Milce, B.J. Orr: J. Chem. Phys. **112**, 9319 (2000); M.A. Payne, A.P. Milce, M.J. Frost, B.J. Orr: Chem. Phys. Lett. **324**, 48 (2000)
86. A.C. Eckbreth: *Laser Diagnostics for Combustion Temperature and Species* (Abacus, Cambridge, Mass. 1988)
87. H. Reisler, M. Noble, C. Wittig: in Molecular Photodissociation Dynamics, ed. by M.N.R. Ashfold, J.E. Baggott (Roy. Soc. Chem., London 1987) pp. 139–176; R. Schinke: Photodissociation Dynamics (Cambridge University Press, UK 1993); H. Finke, H. Spiecker, P. Andresen: J. Chem. Phys. **110**, 4777 (1998)
88. C. Schulz, B. Yip, V. Sick, J. Wolfrum: Chem. Phys. Lett. **242**, 259 (1995)
89. J. Luque, D.R. Crosley: LIFBASE: Database and Spectral Simulation Program (Version 1.5) (SRI International Report MP 99-009, 1999)
90. R.L. Farrow, D.J. Rakestraw, T. Dreier: J. Opt. Soc. Am. B **9**, 1770 (1992) ; R.L. Vander Wal, R.L. Farrow, D.J. Rakestraw: In Twenty-Fourth Symposium (International) on Combustion (The Combustion Institute 1992), pp. 1653–1659; R.B. Williams, P. Ewart, A. Dreizler: Opt. Lett. **19**, 1486 (1994); R.L. Farrow, D.J. Rakestraw: Appl. Phys. B **68**, 741 (1999)
91. J. Wolfrum: In Twenty-Seventh Symposium (International) on Combustion (The Combustion Institute 1998), pp. 1–41; V. Ebert, C. Schulz, H.-R. Volpp, J. Wolfrum, P. Monkhouse: Isr. J. Chem. **39**, 1 (1999)

APPENDIX B:

Y.He and B.J.Orr, "Optical heterodyne signal generation and detection in cavity ringdown spectroscopy based on a rapidly swept cavity," *Chem. Phys. Lett.*, (in press; accepted for publication, 14 December, 2000).

(SEPARATELY ATTACHED)

Optical heterodyne signal generation and detection in cavity ringdown spectroscopy based on a rapidly swept cavity

Yabai He, Brian J. Orr *

Department of Chemistry and Centre for Lasers & Applications

Macquarie University, Sydney, NSW 2109, Australia

Phone: +61 2 9850 8289; Fax: +61 2 9850 8313; Email: brian.orr@mq.edu.au

MS pages (including figures): 14; references: 18 (pp. 9,10); figures & captions: 3 (pp. 11–14)

Submitted to *Chemical Physics Letters*, 23 November 2000;
accepted, 8 December 2000; revised, 11 December 2000;
finally accepted after revision, 14 December 2000.

Abstract

A novel approach to cavity ringdown spectroscopy uses a continuous-wave laser and a rapidly swept optical cavity to shift the frequency of optical radiation stored in the cavity. This frequency-shifted radiation from the ringdown cavity is then combined with incident laser radiation to generate optical heterodyne signals, simply and efficiently. A noise-limited absorbance sensitivity of 3 x 10^{-9} cm^{-1} is realised, using ~35 μW of single-mode radiation from a 1.53-μm tunable diode laser. The resonance properties of a swept optical cavity simplify this heterodyne-detected technique by avoiding the customary need for a fast optical switch or for wavelength-locking of cavity length.

---

* Corresponding author. Fax: +61-2-9850-8313; e-mail: brian.orr@mq.edu.au

1. Introduction

Cavity ringdown laser absorption spectroscopy (CRDS) employs narrowband laser radiation, either pulsed or continuous-wave (cw), for highly sensitive measurements of absorption spectra for a sample contained in a high-finesse optical cavity [1,2]. CRDS with pulsed lasers is straightforward and popular, but cw versions of CRDS are favoured in order to attain superior spectroscopic resolution or to take advantage of cheap, compact tunable diode laser (TDL) sources. In a previous Letter [3], we have demonstrated a novel variant of cw-CRDS, in which the length of the optical cavity is swept, continuously and rapidly, through resonance with narrowband TDL radiation. This facilitates growth and subsequent decay ("ringdown") of optical energy in the cavity and yields absorption spectra with high sensitivity and with minimal instrumental complexity and cost. Our continuously-swept-cavity approach [3] is analogous (but advantageous in some respects) to an earlier cw-CRDS variant [4] in which the ringdown cavity length is rapidly displaced in a single step after the cw laser's wavelength has reached a cavity resonance and its optical energy has built up in the cavity. Each of these methods [3,4] avoids the inherent complexity and expense of an electro-optic or acousto-optic switch, as is needed in more conventional cw-CRDS methods [5–9].

In this Letter, we report a novel optical-heterodyne detected (OHD) extension of cw-CRDS with a rapidly swept ringdown cavity. Our approach is highly sensitive and simple to implement with a commercially available TDL system. In contrast to other more elaborate OHD designs for cw-CRDS [7–9], it does not need a separate optical switch or modulator, nor is it necessary to lock the ringdown cavity length and laser wavelength to each other or to use a laser that is specially stabilised and/or modulated. ***... Please insert Fig. 1 near here***

Fig. 1 depicts our apparatus for OHD cw-CRDS measurements schematically; it is explained progressively throughout this Letter. We start by reviewing some principles of a rapidly swept optical cavity that are intrinsic to our OHD cw-CRDS technique and conclude with a spectroscopic demonstration of the instrumental performance and sensitivity attained.

2. Dynamic response of a rapidly swept optical cavity

Our cw-CRDS approach (OHD or not) is understood in terms of the dynamic response of cw coherent radiation to an optical cavity, the length of which is swept rapidly and continuously by means of a piezoelectric translator (PZT). Ringdown cavities have very high finesse (typically $>10^4$), so that tiny cavity mirror displacements (~1 nm) suffice to shift such cavities on and off resonance. As a cavity mode moves into resonance with the laser wavelength, the cavity transmits much more light because optical energy is built up and stored in it. After the swept cavity has moved off resonance, the input light is effectively blocked by the highly reflective cavity mirrors so that the light stored in the cavity during the build-up period decays gradually with time constant τ; the energy loss rate (*i.e.*, τ^{-1}) depends on the mirror reflectivity and the absorbing medium inside the cavity. The temporal profile of the transmitted light intensity is found [3,4] to be asymmetric, with a slowly decaying tail that exhibits characteristic ringing due to interference of the multiply reflected intra-cavity light.

In our cw-CRDS technique [3], an essential feature (absent in the conventional case of fixed-length ringdown cavities) is the accumulation of Doppler-type frequency shifts $\Delta\nu_j$ that occur with each reflection of intra-cavity radiation from a continuously moving mirror:

$$\Delta\nu_j = (\nu_{j+1} - \nu_j) = \nu_j (2\,v / c), \qquad (1)$$

where ν_j is the frequency of light on its jth round trip in the cavity, v is the mirror velocity, and c is the speed of light. Multiple passes of the cavity therefore generate a narrow distribution of intracavity optical frequency components, each with an amplitude that decays in a manner that follows the change of cavity resonance frequency as the cavity mirror is swept. These intracavity frequency fields interfere with each other and with the (unshifted) incident radiation, producing the modulated cavity ringdown signals that were reported in our previous Letter [3]. For amplitudes of mirror travel and ringdown times that are typical in our experiments, the resulting frequency shifts span the range 0 – 10 MHz (0 – 0.0003 cm^{-1}).

The intracavity optical interference effects that produce such modulated ringdown signals are themselves not newly discovered, as is evident from a recent phasor-based analysis of the time response of a Fabry-Perot interferometer cavity [10]. Such effects have previously been

characterised, both theoretically and experimentally [3,4,10–14], under conditions in which the swept variable is *either* the incident optical frequency (with fixed cavity length) [10,11,14] *or* the optical cavity length (with fixed incident frequency) [3,4,10,12,13].

3. OHD cw-CRDS technique

The Doppler-type frequency shifts outlined in the previous section generate difference frequencies that are intrinsic to the present OHD extension of our original cw-CRDS method. We find that OHD signals can be obtained straightforwardly by monitoring light that emerges through the stationary *front* mirror of the cavity and beating it against incident laser light reflected off that mirror. These two backward co-propagating beams combine on a square-law photodetector (PD_1 in Fig. 1) to yield heterodyne signals at the distribution of Doppler-shifted difference frequencies. Non-OHD cw-CRDS signals are monitored by another photodetector (PD_2) viewing forward-propagating light that is transmitted through the moving *back* cavity mirror, as previously reported [3].

As indicated in Fig. 1, we designate electric radiation fields $\boldsymbol{E}_I$ and $\boldsymbol{E}_B\exp(-t/2\tau)$ that are PD_1-detected portions of the incident laser field ($\boldsymbol{E}_L$) and of the frequency-shifted light transmitted back from the cavity, respectively. The (relatively slow) ringdown decay of the temporal envelope of the latter during the cavity sweep is shown explicitly, but other (relatively rapid) time dependence at optical frequencies is implicitly included in $\boldsymbol{E}_I$ and $\boldsymbol{E}_B$. The OHD CRDS signal $\langle S \rangle$ of interest (detected by PD_1) is then of form:

$$\langle S \rangle \propto |\boldsymbol{E}_I + \boldsymbol{E}_B \exp(-t/2\tau)|^2$$

$$= |\boldsymbol{E}_I|^2 + |\boldsymbol{E}_B|^2 \exp(-t/\tau) + 2\,\mathrm{Re}(\boldsymbol{E}_I^* \bullet \boldsymbol{E}_B)\exp(-t/2\tau). \qquad (2)$$

The time dependence of each of these fields is averaged at optical frequencies by PD_1, but the distribution of Doppler-induced frequency differences between $\boldsymbol{E}_I$ and $\boldsymbol{E}_B$ allows their cross term to appear as a heterodyne signal containing a slowly varying exponential decay factor that depends on the cavity ringdown time τ. More rapidly varying oscillations associated with the $(\boldsymbol{E}_I^* \bullet \boldsymbol{E}_B)$ heterodyne cross term are not shown explicitly in eq. (2). The term in $|\boldsymbol{E}_B|^2$ is comparable to the direct cw-CRDS signal proportional to $|\boldsymbol{E}_F|^2$ that is processed by PD_2, as in

our original non-OHD method [3]. The OHD signal has an advantage in that the field $\boldsymbol{E}_I$ is much stronger than $\boldsymbol{E}_B$ or $\boldsymbol{E}_F$, resulting in a significant amplification factor. Moreover, the OHD signal monitored by PD_1 decays twice as slowly as the direct (PD_2-detected) ringdown signal, thereby further enhancing detection sensitivity. The higher frequency domain of the OHD signal facilitates reduction of low-frequency technical noise by high-pass filtering.

Our OHD approach to cw-CRDS is demonstrated in Figs 2(a) and 2(b), which compare signals measured simultaneously by photodectors PD_2 (direct cw-CRDS) and PD_1 (OHD cw-CRDS), respectively. The cavity length is swept rapidly and continuously by a ramp voltage applied to the PZT that bears one of the mirrors. The forward-transmitted signal from PD_2, shown in Fig. 2(a), builds up and peaks just after the exact resonance point (at t = 0 on the abscissa) between the cavity and the laser wavelength. The optical cavity then moves out of resonance and oscillations set in, with their period and depth of modulation decreasing as time delay increases. The decay envelope depends on the energy loss rate of the cavity and can be used for direct cw-CRDS measurements [3]. The OHD ringdown signal, shown in Fig. 2(b), contains information about the amplitudes and relative phase of the optical fields $\boldsymbol{E}_I$ and $\boldsymbol{E}_B$ that are monitored by PD_1 at a narrow distribution (typically ~1 MHz FWHM) of Doppler-shifted difference frequencies, as outlined above. ***... Please insert Fig. 2 near here***

The observations shown in Figs 2(a and b) are in excellent agreement with corresponding numerical simulations performed by superposing multiply reflected cw laser radiation in a rapidly swept optical cavity. Our simulation of Fig. 2(a) parallels several previous studies [3,4,10–14]. In the case of Fig. 2 (b), our simulations and observations are qualitatively similar to earlier results for frequency-swept [10, 14] and cavity-swept [10] ringdown effects.

For useful OHD cw-CRDS measurements, it is necessary to extract the ringdown decay rate τ^{-1} from the PD_1 signal. One possible approach would be to fit features of OHD waveforms, such as that in Fig. 2(b), to a model-derived function. A more efficient method, capable of implementation in real time while an absorption spectrum is being recorded, entails pre-processing signals from PD_1 by analog electronic circuits that rectify and smooth the oscillatory part of the ringdown decay, using a multiplier and low-pass filter. The latter method has been used here, as illustrated in Fig. 2(c); it yields a smooth, single-exponential

decay "tail" from which a ringdown time τ can be rapidly and accurately derived. Likewise, PD_2-detected, forward-transmitted cw-CRDS measurements can be made as before [3].

4. OHD cw-CRDS apparatus

Our cw-CRDS apparatus has already been illustrated in Fig. 1. It comprises a cw external-cavity TDL (New Focus model 6262/6200; ~5 mW single-mode output; tunable over 1.50 – 1.59 μm with ~1-MHz optical bandwidth), a piezoelectrically controlled ringdown cavity, two amplified photodetectors (PD_1, PD_2; InGaAs; 125-MHz bandwidth), a digital oscilloscope (Tektronix TDS3000 series; bandwidth, 200 – 500 MHz), and control electronics with IEEE-488 computer interface. The TDL beam traverses an optical isolator (–80 dB) and is mode-matched to the ringdown cavity by a lens of 50-cm focal-length. A polarisation control unit, comprising one of the 45° Faraday rotators that forms part of the optical isolation system, enables a polarising beam splitter (PBS) to direct the backward-propagating light fields $\boldsymbol{E}_I$ and $\boldsymbol{E}_B$ to the OHD photodetector PD_1. This configuration makes efficient use of available laser power for OHD measurements. Photodetector PD_2 monitors the direct CRDS signal forward-transmitted by the ringdown cavity, which comprises two concave mirrors (>99.96% reflectivity, –1-m radius, 45 cm apart) mounted in an evacuable optical cell fitted with electronic manometers. A cylindrical low-voltage PZT (driven by a ramp with ~10-V amplitiude) allows the ringdown cavity length to be swept with amplitude of ~1.6 μm at frequencies up to ~1 kHz. A synchronous gate selects the portion of signal output from PD_1 and/or PD_2 around the midpoint of each positive-going sweep, where the velocity of the cavity mirror is constant (typically ~1 mm s^{-1}). The digital oscilloscope is level-triggered by the ringdown signal, since cavity resonances occur at points in the sweep cycle that vary as the input TDL wavelength is scanned. Successive ringdown curves are collected at a rate of ~500 Hz and averaged in the oscilloscope, with a dead time of ~0.1 s during which a ringdown time τ is extracted from the averaged waveform (typically over the range $5 < t < 15$ μs) and the TDL wavelength is incremented (in steps of ~0.01 nm for a coarse scan or ~0.4 pm for a fine scan).

5. Spectroscopic performance and sensitivity

As a spectroscopic demonstration of this OHD cw-CRDS technique with a rapidly swept cavity, we have examined a rovibrational absorption band of carbon dioxide gas (CO_2) at ~1.53 μm, which is covered by the HITRAN'96 database [15]. This band is extremely weak and is difficult to detect by conventional infrared spectroscopy, even in a long-path absorption cell. Fig. 3 shows a cw-CRDS trace, recorded for CO_2 at 50 mbar. At each wavelength step, 256 build-up-and-decay curves are averaged by the digital oscilloscope and the decay rate is averaged a further 8 times by computer; this requires a dwell time of ~5 s for each 50-MHz (0.0017-cm^{-1}) step in the finely scanned spectrum. ***... Please insert Fig. 3 near here***

Prominent features of the spectrum, labeled with corresponding rotational quantum numbers $J = 2 - 14$, belong to the Q branch of the 6538-cm^{-1} $(11^12)_{II} \leftarrow 00^00$ rovibrational band [15,16]. (Here, odd-J features are forbidden by nuclear-spin statistics and the $J = 0$ component is missing since the vibrational angular momentum l equals 1 in the upper vibrational state.) Three other labeled peaks in the same spectral region are assigned [15,16] as follows: **a**, 6538.02-cm^{-1} R(6) line of the $(40^01)_I \leftarrow (10^00)_I$ band; **b**, 6537.99-cm^{-1} R(1) line of the $(31^11)_I \leftarrow 01^10$ band; **c**, 6537.29-cm^{-1} R(50) line of the $(30^01)_I \leftarrow 00^00$ band. Several other unlabeled features have not previously been observed (to our knowledge) and are tentatively attributed to isotopic species of CO_2 (*e.g.*, $^{13}CO_2$) and/or ultra-weak hot bands.

Fig. 3 was recorded with the incident TDL optical power attenuated 100-fold to ~35 μW to avoid saturation of the very sensitive low-noise preamplifier associated with PD_1. From such observations, we deduce a noise-limited sensitivity for absorbance detection of 3×10^{-9} cm^{-1} and an estimated dynamic range of at least 35 dB (*i.e.*, a factor of 3000). These performance figures are markedly superior to those obtained (7×10^{-8} cm^{-1} and ~20 dB) in our previous CRDS measurements with cw [3] or pulsed [17] lasers. They compare favourably (within an order of magnitude) with other OHD cw-CRDS studies [7,8,9], obtained with much more elaborate instrumentation. Advanced noise-immune OHD FM-spectroscopic techniques, with a sensitivity of 1×10^{-14} cm^{-1} [18], represent the state of the art in this field.

6. Concluding remarks

Our use of a rapidly swept cavity for OHD cw-CRDS measurements yields high spectroscopic resolution, accuracy, and sensitivity. We foresee further technical improvements, without sacrificing our technique's intrinsic simplicity, low cost, and compactness. Such instrumental developments might include: a lower-gain, low-noise photodetector to take advantage of the full 5-mW power of the TDL; replacing the present continuous cavity-scan scheme [3] by more abrupt mirror displacement [4] of well-defined amplitude that would shift the effective OHD difference frequency regime further above that of low-frequency technical noise; optical-fiber coupling to allow the ringdown cavity to be remotely located relative to the TDL and detection system, thereby facilitating industrial and environmental sensing applications.

Acknowledgments

This research was supported by grants from the Australian Research Council and Macquarie University.

References

[1] J. J. Scherer, J. B. Paul, A. O'Keefe, R. J. Saykally, Chem. Rev. 97 (1997) 25, and references therein.

[2] K. W. Busch and M. A. Busch, eds, Cavity-Ringdown Spectroscopy – An Ultratrace-Absorption Measurement Technique, ACS Symposium Series No. 720 (American Chemical Society, Washington, DC, 1999).

[3] Y. He, B. J. Orr, Chem. Phys. Lett. 319 (2000) 131.

[4] J. W. Hahn, Y. S. Yoo, J. Y. Lee, J. W. Kim, H.-W. Lee, Appl. Opt. 38 (1999) 1859.

[5] D. Romanini, A. A. Kachanov, N. Sadeghi, F. Stoeckel, Chem. Phys. Lett. 264 (1997) 316.

[6] Y. He, M. Hippler, M. Quack, Chem. Phys. Lett. 289 (1998) 527.

[7] M. D. Levenson, B. A. Paldus, T. G. Spence, C. C. Harb, J. S. Harris, R. N. Zare, Chem. Phys. Lett. 290 (1998) 335.

[8] M. D. Levenson, B. A. Paldus, T. G. Spence, C. C. Harb, R. N. Zare, M. J. Lawrence, R. L. Byer, Opt. Lett. 25 (2000) 920.

[9] J. Ye, J. L. Hall, Phys. Rev. A 61 (2000) 061802.

[10] M. J. Lawrence, B. Wilke, M. E. Husman, E. K. Gustafson, R. L. Byer, J. Opt. Soc. Am. B 16 (1999) 523.

[11] Z. Li, R. G. T. Bennett, G. E. Stedman, Optics Comm. 86 (1991) 51.

[12] K. An, C. Yang, R. R. Dasari, M. S. Feld, Opt. Lett. 20 (1995) 1068.

[13] J. Poirson, F. Bretenaker, M. Vallet, A. Le Floch, J. Opt. Soc. Am. B 14 (1997) 2811.

[14] J. Ye, L.-S. Ma, J. L. Hall, in: Chapter 15 of ref. [2], pp. 233–253.

[15] L. S. Rothman, C. P. Rinsland, A. Goldman, S. T. Massie, D. P. Edwards, J.-M. Flaud, A. Perrin, C. Camy-Peyret, V. Dana, J.-Y. Mandin, J. Schroeder, A. McCann, R. R. Gamache, R. B. Wattson, K. Yoshino, K. V. Chance, K. W. Jucks, L. R. Brown, V. Nemtchinov, P. Varanasi, J. Quant. Spectrosc. Radiat. Transfer 60 (1998) 665.

[16] L. S. Rothman, R. L. Hawkins, R. B. Wattson, R. R. Gamache, J. Quant. Spectrosc. Radiat. Transfer 48 (1992) 537.

[17] G. W. Baxter, M. A. Payne, B. D. W. Austin, C. A. Halloway, J. G. Haub, Y. He, A. P. Milce, J. F. Nibler, B. J. Orr, Appl. Phys. B 71 (2000) 651.

[18] J. Ye, L.-S. Ma, J. L. Hall, J. Opt. Soc. Am. B 15 (1998) 6.

Figure captions

Fig. 1. Schematic of the apparatus for optical-heterodyne detected (OHD) cavity ringdown spectroscopy with a continuous-wave tunable diode laser and a rapidly swept ringdown cavity. Two photodetectors, PD_1 and PD_2, monitor the OHD (back-scattered, "$\boldsymbol{E}_I + \boldsymbol{E}_B$") and direct (forward-scattered, "$\boldsymbol{E}_F$") ringdown signals, respectively, as explained in sections 3 and 4. Other essential features of the apparatus are a high-finesse optical cavity, the length of which is swept rapidly and continuously by means of a piezoelectric translator (PZT), and (in the OHD case) a polarisation control unit incorporating a polarising beam splitter (PBS) that directs the "$\boldsymbol{E}_I + \boldsymbol{E}_B$" light fields to photodetector PD_1.

Fig. 2. Simultaneously recorded cw-CRDS signals showing the dynamic response of cw coherent radiation in a rapidly swept optical cavity. Trace (a) is the forward-scattered signal directly monitored [3] by photodetector PD_2, as explained in section 2. An explanation is given in section 3 of trace (b), which is the raw OHD signal registered by photodetector PD_1, and of trace (c), the corresponding rectified and filtered waveform from which a cavity ringdown time τ can be extracted.

Fig. 3. OHD cw-CRDS measurements around 1.53 μm of CO_2 gas at 50 mbar in a rapidly swept optical cavity. The spectrum records very weak rovibrational absorption bands of CO_2, including the Q(J) features of the 6538-cm^{-1} $(11^12)_{II} \leftarrow 00^00$ band, with $J = 2 - 14$. Rovibrational assignments of peaks a, b, c and other features in the spectrum, guided by the HITRAN'96 database [15,16], are discussed in section 5. The observed noise level corresponds to a sensitivity of 3×10^{-9} cm^{-1} for absorption detection; the estimated dynamic range for linear detection is 35 dB.

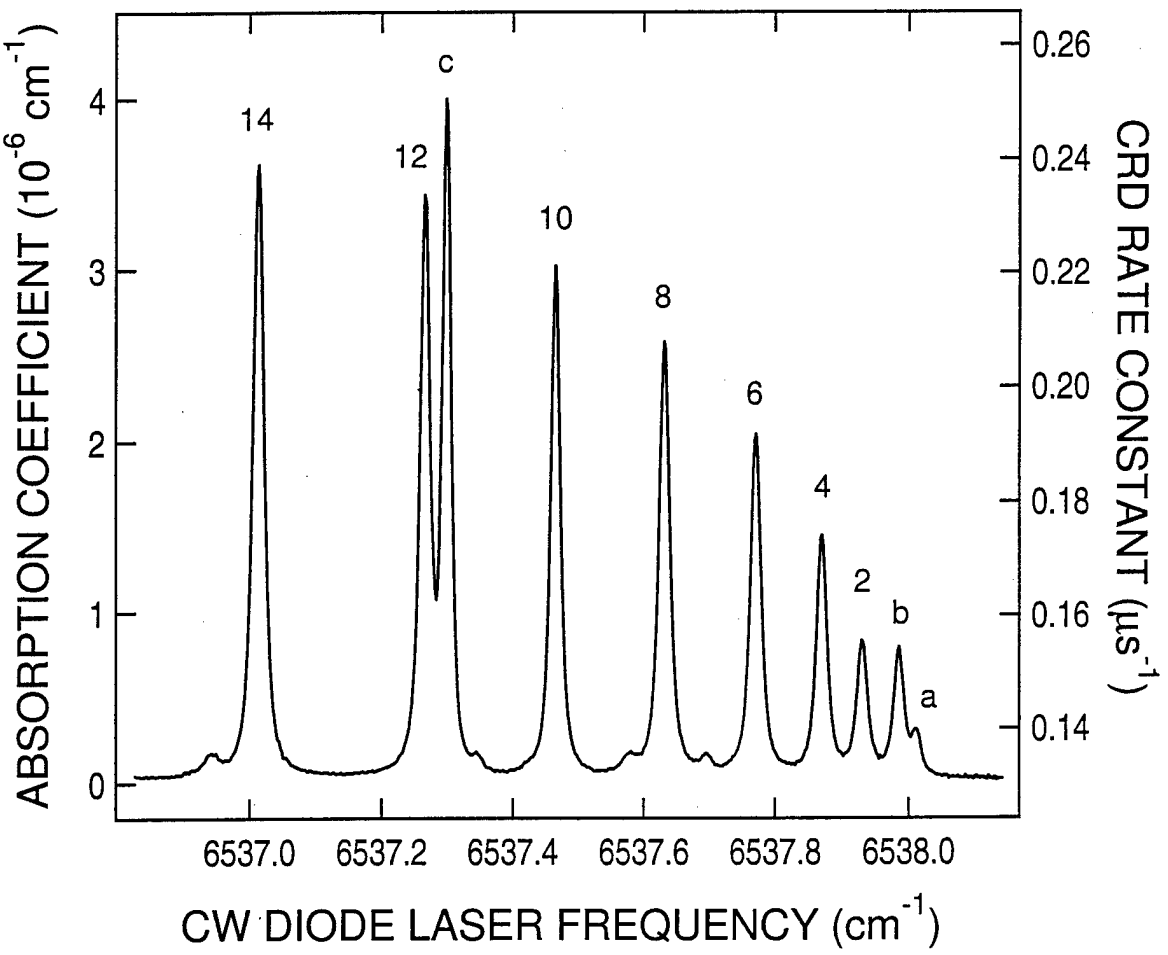

Fig. 3. OHD cw-CRDS measurements around 1.53 μm of CO_2 gas at 50 mbar in a rapidly swept optical cavity. The spectrum records very weak rovibrational absorption bands of CO_2, including the Q(J) features of the 6538-cm^{-1} $(11^12)_{II} \leftarrow 00^00$ band, with J = 2 – 14. Rovibrational assignments of peaks a, b, c and other features in the spectrum, guided by the HITRAN'96 database [15,16], are discussed in section 5. The observed noise level corresponds to a sensitivity of 3 x 10^{-9} cm^{-1} for absorption detection; the estimated dynamic range for linear detection is 35 dB.